

Spectral Theory of Non-Markovian Dissipative Phase Transitions

Baptiste Debecker, John Martin, François Damanet¹

¹*Institut de Physique Nucléaire, Atomique et de Spectroscopie,
CESAM, University of Liège, B-4000 Liège, Belgium*

(Dated: April 10, 2024)

Controlling phase transitions in quantum systems via coupling to reservoirs has been mostly studied for idealized (memory-less) environments. Here, we present a general method to tackle dissipative phase transitions (DPTs) in non-Markovian systems, extending the scope of dissipative engineering of matter phases to more realistic materials and experiments in the solid-state and atomic, molecular and optical physics. We show how memory effects can be used to reshape phase boundaries but also reveal the existence of DPTs genuinely triggered by non-Markovianity.

Introduction. Finding new ways to control phase transitions in quantum systems to access desired properties is at the forefront of research for developing new materials and technologies. In this context, driven-dissipative mechanisms obtained via the coupling of systems to engineered environments and fields offer opportunities to generate matter phases otherwise inaccessible [1–3].

However, thus far, dissipative phase transitions (DPTs), which have been observed in controlled experiments [4–9], have mostly garnered theoretical attention in systems coupled to memoryless reservoirs [10–12]. Yet, most realistic systems are coupled to reservoirs with a spectral structure [13], giving the latter a memory of past system-bath exchanges, which considerably complicates their dynamics. Such non-Markovian effects are crucial to be understood, not least because they can be used as a resource to generate useful phenomena, such as non-Markovian-assisted steady state entanglement [14], quantum transport [15], spin squeezing [16], chaotic behaviors [17] or new dynamical phases [18]. Moreover, from a computational perspective, it is sometimes desirable to derive reduced descriptions of a large Markovian open quantum system in order to deal with a smaller Hilbert space, which usually implies dealing with non-Markovian effects [19, 20].

Here, we extend the spectral theory of DPTs to non-Markovian systems and present a general method to characterize their signatures, opening possibilities for exploring DPTs in a wider range of systems. Our approach is based on the Hierarchical Equations of Motion (HEOM) [21–26], a numerical method for non-Markovian dynamics extensively used in quantum physics and chemistry, from which one can define a generalization of the Liouvillian usually associated with the Lindblad master equation for Markovian systems whose spectral properties are connected to DPTs. One of the necessary conditions for DPTs is the closing of the Liouvillian gap [10]: Here we show how to define a similar quantity for non-Markovian systems.

Non-Markovian effects in DPTs have been studied via other techniques [27–30], but mostly only on the paradigmatic spin-boson model [31–33]. As our approach is

the natural extension of the powerful spectral machinery widely used for Markovian systems, it provides an ideal framework to explore non-Markovian effects in new regimes and for more realistic systems and experiments.

Below, we first present the generalization of the Liouvillian for non-Markovian systems and derive its properties and connections with DPTs and symmetries. As examples of applications, we first study a generalized Lipkin-Meshkov-Glick model [34] and show that deviations from a Markovian reservoir lead to a shift of the phase transition boundary. Then, even more remarkably, we reveal the existence of DPTs that only appear in the non-Markovian regime.

Theoretical framework. Consider a system S coupled to a bosonic environment E at zero temperature [35]. The total Hamiltonian ($\hbar = 1$) is

$$H = H_S + \underbrace{\sum_k \omega_k a_k^\dagger a_k}_{\equiv H_E} + \underbrace{\sum_k (g_k a_k L_k^\dagger + g_k^* a_k^\dagger L_k)}_{\equiv H_{\text{int}}}, \quad (1)$$

where H_S (H_E) is the system (environment) Hamiltonian, with a_k (a_k^\dagger) the annihilation (creation) operator for the k -th mode of frequency ω_k , and H_{int} is the interaction Hamiltonian with L_k being arbitrary system operators and g_k being the system-bath coupling strengths. The effect of the environment on the system is encoded in the spectral density $J(\omega) = \pi \sum_k |g_k|^2 \delta(\omega - \omega_k)$ or equivalently in the bath correlation function $\alpha(\tau) = \sum_k |g_k|^2 e^{-i\omega_k \tau} = (1/\pi) \int_0^\infty J(\omega) e^{-i\omega \tau} d\omega$. We assume that the correlation function, which depends on the model, is a sum of M decaying exponentials

$$\alpha(\tau) = \sum_{j=1}^M G_j e^{-i\omega_j \tau - \kappa_j |\tau|}, \quad \kappa_j, \omega_j \in \mathbb{R}, G_j \in \mathbb{C}. \quad (2)$$

This decomposition, which is not unique [36], can be performed either exactly or with great precision in a wide range of situations [25, 37–39]. For $G_j \in \mathbb{R}$, this amounts to decompose the non-Markovian environment E into a set of M modes of frequencies $\{\omega_j\}$ which are damped with rates $\{\kappa_j\}$ due to their coupling to independent Markovian baths, as illustrated in Fig. 1. This pseudo-

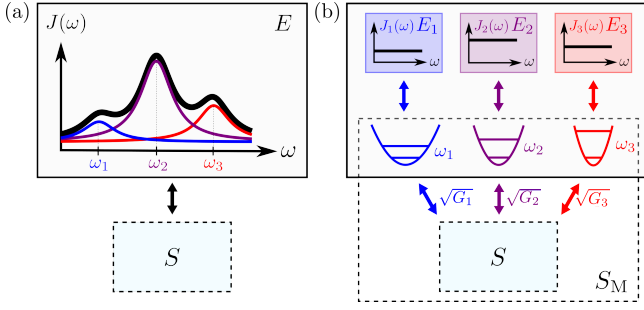


FIG. 1. (a): Sketch of a system S interacting with a structured environment E characterized by a spectral density $J(\omega)$ that can be decomposed into three Lorentzians, as if the system was coupled to three pseudo-modes coupled to their own unstructured bath (b). If one enlarges the system S by including the pseudo-modes (system S_M in the dashed black box), the dynamics can be treated by a Lindblad description.

mode picture [40–47] is relevant for atoms in cavities, superconducting qubits coupled to resonators [48, 49], electrons-phonon systems [50, 51], or emitters in plasmonic cavities [52]. Using complex G_j is even more general and allows for instance an efficient fit of Ohmic spectral density [36, 53] and the study of critical behaviors [54].

When the global system is initially in the state $\rho(0) = \rho_S(0) \otimes \rho_B(0)$, the exact dynamics of S can be described by the HEOM method which takes the form [21–25]

$$\begin{aligned} \frac{d\rho^{(\vec{n}, \vec{m})}}{dt} = & -i[H_S, \rho^{(\vec{n}, \vec{m})}] - (\vec{w}^* \cdot \vec{n} + \vec{w} \cdot \vec{m})\rho^{(\vec{n}, \vec{m})} \\ & + \sum_{j=1}^M \left\{ G_j n_j L_j \rho^{(\vec{n} - \vec{e}_j, \vec{m})} + G_j^* m_j \rho^{(\vec{n}, \vec{m} - \vec{e}_j)} L_j^\dagger \right. \\ & \left. + [\rho^{(\vec{n} + \vec{e}_j, \vec{m})}, L_j^\dagger] + [L_j, \rho^{(\vec{n}, \vec{m} + \vec{e}_j)}] \right\}, \quad (3) \end{aligned}$$

with $\vec{n} = (n_j)$ and $\vec{m} = (m_j)$ multi-indices in \mathbb{N}^M , $\vec{w} = (\kappa_j + i\omega_j) \in \mathbb{C}^M$, $\vec{e}_j = (\delta_{jj'})$ unit vectors, and $\vec{a} \cdot \vec{b} = \sum_j a_j^* b_j$ the inner product on \mathbb{C}^M , and L_j the system operator coupled to the j^{th} pseudo mode. In Eq. (3), $\rho^{(\vec{0}, \vec{0})} \equiv \rho_S$ corresponds to the physical density operator of the system S with which all the mean values of system observables are computed, while $\rho^{(\vec{n}, \vec{m})}$ for $(\vec{n}, \vec{m}) \neq (\vec{0}, \vec{0})$, which are also operators acting on the system space, correspond to auxiliary states from which bath correlations can be obtained [16]. Although the hierarchy is formally infinite, it can be truncated at large hierarchy depth indices \vec{n} and \vec{m} . In practice, the stronger the non-Markovianity, the larger the number of auxiliary states we need to retain to obtain convergence of the results. Here, we choose the triangular truncation $\rho^{(\vec{n}, \vec{m})} = 0 \forall \vec{n}, \vec{m} : \sum_j (n_j + m_j) > k_{\text{max}}$, where k_{max} is the truncation order, yielding a total of $K = (2M + k_{\text{max}})! / ((2M)! k_{\text{max}}!)$ auxiliary states [16].

By stacking in a vector $|\rho\rangle\rangle$ all the vectorized versions

of the matrices $\rho^{(\vec{n}, \vec{m})}$, Eq. (3) can be written in the form

$$\frac{d|\rho\rangle\rangle}{dt} = \mathcal{L}_{\text{HEOM}}(k_{\text{max}}) |\rho\rangle\rangle, \quad (4)$$

where $\mathcal{L}_{\text{HEOM}}(k_{\text{max}})$ is the *HEOM Liouvillian*, the generator of the non-Markovian dynamics of the system, exact for $k_{\text{max}} \rightarrow +\infty$ and which generalises Lindblad’s Liouvillian (see Supplemental Material (SM) for an example). Instead of using $\mathcal{L}_{\text{HEOM}}$, one can sometimes as noted above enlarge the system by including explicit pseudo-mode degrees of freedom damped by standard Lindblad decay channels, as illustrated in Fig. 1(b). This would define a Markovian Liouvillian \mathcal{L}_M for the global system S_M . However, using $\mathcal{L}_{\text{HEOM}}$ is computationally more favorable than \mathcal{L}_M , especially for large M (see SM).

Properties of the HEOM Liouvillian. The superoperator $\mathcal{L}_{\text{HEOM}}$ is linear and in general non-Hermitian. We assume it is diagonalizable and denote its eigenvectors and eigenvalues by $|\rho_i\rangle\rangle$ and λ_i . For a truncation order k_{max} , its dimension is $D = K \dim(\mathcal{H}_S)^2$. It admits the following properties (see proofs in the SM): (i) its spectrum is symmetric with respect to the real axis; (ii) it preserves the trace of the physical state $\rho^{(\vec{0}, \vec{0})}$; (iii) the eigenvalue 0 is always in its spectrum, guaranteeing the existence of a stationary state; (iv) all the eigenvalues must have a negative real part in the limit $k_{\text{max}} \rightarrow +\infty$; (v) $\text{Tr}[\mathbf{1}^{(\vec{0}, \vec{0})} \rho_i] = 0$ with $\mathbf{1}^{(\vec{0}, \vec{0})}$ the projector onto the physical state space if ρ_i is a right eigenoperator of $\mathcal{L}_{\text{HEOM}}$ associated with the eigenvalue λ_i with $\text{Re}[\lambda_i] \neq 0$. As in [10, 11], we order the eigenvalues of $\mathcal{L}_{\text{HEOM}}$ so that $|\text{Re}[\lambda_0]| < |\text{Re}[\lambda_1]| < \dots < |\text{Re}[\lambda_D]|$, where $\lambda_0 = 0$.

DPT and HEOM Liouvillian spectrum. Consider a system described by Eq. (4) which admits a valid thermodynamic limit $N \rightarrow \infty$ and a unique steady state ρ_{ss} for all finite N . We say that the system undergoes a phase transition of order M when a non-analytical change in a g -independent system observable O occurs when the parameter g tends to a critical value g_c for $N \rightarrow \infty$, i.e., [10]

$$\lim_{g \rightarrow g_c} \left| \frac{\partial^M}{\partial g^M} \lim_{N \rightarrow +\infty} \langle O \rangle_{ss} \right| = +\infty, \quad (5)$$

where $\langle O \rangle_{ss} = \text{Tr}[O \rho_{ss}^{(\vec{0}, \vec{0})}]$. This definition of DPTs is the same as for Markovian systems. The only difference is that the steady state is now obtained from the HEOM Liouvillian (4). Like for the Markovian case, a non-analytical change as described by (5) must occur due to a level crossing in the spectrum of $\mathcal{L}_{\text{HEOM}}$, which implies the closing of the HEOM Liouvillian gap $\text{Re}[\lambda_1]$. For 1st-order DPTs, the connection is even stronger as a DPT occurs *iff* $\text{Re}[\lambda_1] = 0$ at $g = g_c$ and $\text{Im}[\lambda_1] = 0$ in a finite domain around g_c for $N \rightarrow \infty$ (see SM).

Symmetries and DPTs. We call *weak symmetry* of $\mathcal{L}_{\text{HEOM}}$ any unitary superoperator \mathcal{U} such that $[\mathcal{L}_{\text{HEOM}}, \mathcal{U}] = 0$. The matrix representing $\mathcal{L}_{\text{HEOM}}$ in the

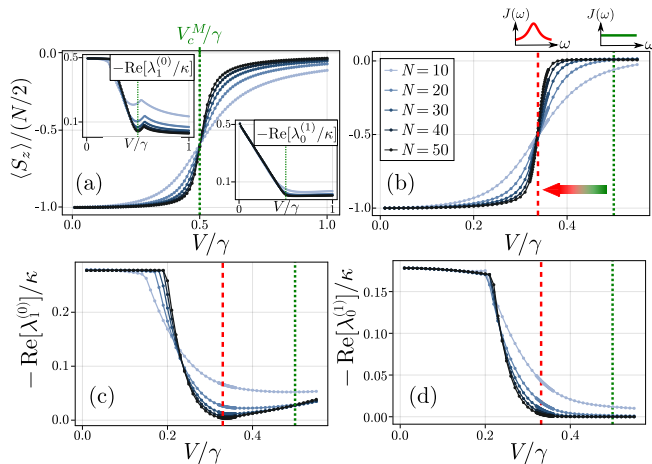


FIG. 2. Signatures of the 1st-order DPT for the generalized dissipative LMG model (6) obtained from $\mathcal{L}_{\text{HEOM}}$, showing how environmental spectral structures affect the DPT. (a,b): Steady state magnetization $\langle S_z \rangle$ as a function of V/γ for $\kappa/\omega = 50$ (a) and $\kappa/\omega = 1$ (b). The vertical green and red dashed lines indicate the transitions points for $\kappa/\omega = 50$ and 1, respectively. (c,d): Liouvillian gap $-\text{Re}[\lambda_1^{(0)}]$ (c) and $-\text{Re}[\lambda_0^{(1)}]$ (d) as a function of V/γ , indicating respectively the DPT and the SSB associated with the DPT. The insets of (a) show the same quantities for the Markovian case. Truncation orders are $k_{\text{max}} = 2$ (a) and $k_{\text{max}} = 6$ ($N = 10-30$), 7 ($N = 40$), 9 ($N = 50$) (b-d).

eigenvector basis of \mathcal{U} is block-diagonal, i.e., $\mathcal{L}_{\text{HEOM}} = \bigoplus_{u_k} \mathcal{L}_{u_k}$, where each block \mathcal{L}_{u_k} is associated with distinct eigenvalues u_k of \mathcal{U} where $k \in \{0, 1, \dots\}$. We define the *symmetry sector* L_{u_k} as the subspace spanned by the eigenvectors of \mathcal{U} associated with the eigenvalue u_k . We can prove, in close analogy with the Markovian case [10] that if the steady-state $|\rho_{ss}\rangle\rangle$ of (4) is unique, then $|\rho_{ss}\rangle\rangle \in L_{u_0=1}$ [55]. A spontaneous symmetry breaking (SSB) corresponds to the emergence of a zero eigenvalue in each symmetry sectors k in the limit $N \rightarrow \infty$. To be specific, if $\mathcal{L}_{\text{HEOM}}$ is a direct sum of $n+1$ blocks and if its eigenvalues are sorted in each block k as $|\text{Re}[\lambda_0^{(k)}]| < |\text{Re}[\lambda_1^{(k)}]| < \dots$, a SSB is signaled by $\lambda_0^{(k)} \rightarrow \lambda_0^{(0)} = 0 \forall k > 0$ for $g \geq g_c, N \rightarrow +\infty$ [56]. This means that the independent hierarchies associated with each block k mix in the limit $N \rightarrow +\infty$ so that steady-states that explicitly break the symmetry emerge.

1st-order DPT. We first illustrate our approach for a Lipkin-Meshkov-Glick (LMG) model of the form

$$H_{\text{LMG}} = \frac{V}{N} (S_x^2 - S_y^2) = \frac{V}{2N} (S_+^2 + S_-^2), \quad (6)$$

where $S_\alpha = \sum_{j=1}^N \sigma_\alpha^{(j)}/2$ ($\alpha = x, y, z$) are the collective spin operators defined in terms of single-spin Pauli operators $\sigma_\alpha^{(j)}$ and $S_\pm = S_x \pm iS_y$. When the spin system undergoes collective decay as described by Lindblad's mas-

ter equation

$$\dot{\rho} = -i[H_{\text{LMG}}, \rho] + \frac{\gamma}{2N} \mathcal{D}[S_-] \quad (7)$$

where $\mathcal{D}[o] = 2o\rho o^\dagger - \{o^\dagger o, \rho\}$, as would occur if coupled to an unstructured bath with $\alpha(\tau) = (\gamma/N)\delta(\tau)$, the model exhibits a 1st-order DPT at the critical point $V_c^M = \gamma/2$ [34], separating a steady state phase where $\langle S_z \rangle \rightarrow -N/2$ ($V < V_c^M$) to a phase where $\langle S_z \rangle \rightarrow 0$ ($V > V_c^M$) for $N \rightarrow \infty$, as can be seen in Fig. 2(a). Here, we generalize the study of this DPT to the non-Markovian regime by considering a finite memory time for the bath with a correlation function of the form $\alpha(\tau) = G e^{-\kappa|\tau| - i\omega\tau}$, as if the damping of the collective spin was originating from the coupling of the system to a *structured* bath via an interaction Hamiltonian $H_{\text{int}} = \sqrt{G}(S_- a^\dagger + S_+ a)$ with $G = \gamma\kappa/(2N)$ and a the annihilation operator of a damped pseudo-mode of Hamiltonian $H_E = \omega a^\dagger a$. This model allows us to study non-Markovian effects on the DPT and compare them to the Markovian case by tuning the “loss” rate κ of the pseudo mode. Indeed, the collective spin and the pseudo mode form an extended Markovian system governed by the master equation

$$\dot{\rho}_{\text{tot}} = -i[H, \rho_{\text{tot}}] + \kappa \mathcal{D}[a] \quad (8)$$

with $H = H_{\text{LMG}} + H_E + H_{\text{int}}$. Adiabatic elimination of the pseudo-mode's degrees of freedom recovers Eq. (9) in the limit $\kappa \rightarrow \infty$ (see SM), as expected since $\alpha(\tau) \rightarrow (\gamma/N)\delta(\tau)$ for $\kappa \rightarrow \infty$. When κ is finite, memory effects arise and affect the DPT as described below. Note that Eq. (8) has a \mathbb{Z}_2 symmetry represented by $\mathcal{U}_2 = U_2 \otimes U_2^\dagger$ with $U_2 = e^{i\pi(S_z + a^\dagger a)}$. \mathcal{U}_2 has two distinct eigenvalues $u_k = e^{ik\pi} = \pm 1$ with $k = 0, 1$, so there are two symmetry sectors, with $L_{k=0}$ containing ρ_{ss} .

The impact of memory effects on the DPT based on $\mathcal{L}_{\text{HEOM}}$ for the spin system can be seen in Fig. 2. First, we see in panel (b) that the steady state spin magnetization $\langle S_z \rangle$ exhibits a sharp transition at a critical point smaller than in the Markovian case shown in Fig. 2(a). This demonstrates that deviations from a flat spectral density can reshape phase boundaries. A mean-field analysis of (8) shows that the shift in the critical point increases as κ decreases (see SM for all details). Physically, this can be understood as follows: the smaller κ , the greater the probability that excitations escaping from the system will be reabsorbed at later times. The degree of openness of the system therefore decreases as κ decreases, which leads to a stabilisation of the phase dominated by the Hamiltonian (6) for small V . For $\kappa \rightarrow 0$ (i.e., for a closed system), the phase transition disappears because the Hamiltonian dynamics no longer competes with dissipative dynamics. In the opposite limit $\kappa \rightarrow \infty$, we recover the Markovian case. The HEOM Liouvillian spectrum correctly captures all DPT signatures. Indeed,

it captures the emergence of both the level-touching at the critical point in the symmetry sector $k = 0$, i.e., $-\text{Re}[\lambda_1^{(0)}] \rightarrow 0$ as $N \rightarrow \infty$ and the SSB associated to the DPT, i.e., $-\text{Re}[\lambda_0^{(1)}] \rightarrow 0$ for V above the critical point as $N \rightarrow \infty$, as can be seen in panels (c) and (d).

Note that this DPT cannot be studied via an approximate reduced description of the spin dynamics obtained after adiabatic elimination of the pseudo-mode, as the related mean-field approach predicts qualitatively different steady states (see SM). In general, reduced descriptions cannot account for all the features of a DPT and can even fail to capture DPTs, as elaborated on further below and strongly motivates again the use of our framework.

2nd-order DPT. The second model we consider, also experimentally relevant for cavity QED [57], is of the form (1) with $H_S = H_{\text{LMG}} + hS_z$ and $L_k \equiv L = S_x$. For an unstructured bath with $\alpha(\tau) = \gamma\delta(\tau)$, the system dynamics is governed by the master equation

$$\dot{\rho} = -i[H_{\text{LMG}} + hS_z, \rho] + \frac{\gamma}{2N}\mathcal{D}[S_x] \quad (9)$$

whose unique steady-state is the maximally mixed state $\rho_{\text{ss}} \propto \mathbb{1}_{N+1}$, preventing the emergence of any DPT. However, if we add again a realistic finite memory time for the bath by considering $\alpha(\tau) = (\gamma\kappa/2)e^{-i\omega\tau - \kappa|\tau|}$, we unveil the existence of two consecutive 2nd-order DPTs separating three different phases upon varying the squeezing strength V . This can be seen in Fig. 3, where we show that our approach captures all the features of the DPTs in agreement with mean-field predictions detailed in the SM. Panels (a-c) show the steady states expectations $\langle S_z \rangle$ and $\langle S_y^2 \rangle$ as a function of V , which distinguish the phases [labeled as (I), (II) and (III)], as we have $\langle S_y^2 \rangle = 0$ in phases (I) and (II) and $\langle S_z \rangle = -N/2$ in phase (II) only. In addition, as there is a \mathbb{Z}_2 symmetry represented by \mathcal{U}_2 in our model akin to the symmetry that is broken in the DPT of the Dicke model [19], we expect a SSB manifesting as $\lambda_0^{(1)} \rightarrow 0$ as $N \rightarrow +\infty$ in phases (I) and (III), accompanied by an exponential closure of the gap [20]. This behavior is illustrated in panels (b) and (d). Also, note that as the critical points are at $V = -h + \gamma\kappa\omega/[2(\kappa^2 + \omega^2)]$ and $V = h$, taking the limit $\kappa \rightarrow \infty$ does not recover the prediction of the Lindblad scenario, i.e., no DPT. In other words, we have $\lim_{\kappa \rightarrow \infty} \lim_{N \rightarrow \infty} \neq \lim_{N \rightarrow \infty} \lim_{\kappa \rightarrow \infty}$. Physically, taking $\kappa \rightarrow \infty$ amounts to consider equal absorption and emission rates for the system, pushing it inevitably to the infinite temperature state. Considering a finite κ restores a memory for the bath, i.e., a system-frequency-dependent response, thereby providing the necessary competition between Hamiltonian and dissipative dynamics for the emergence of DPTs.

Other model. We have also employed our method in the case of a challenging $\mathbb{U}(1)$ -symmetric two-mode Dicke model [20, 58] to capture both the correct steady-state

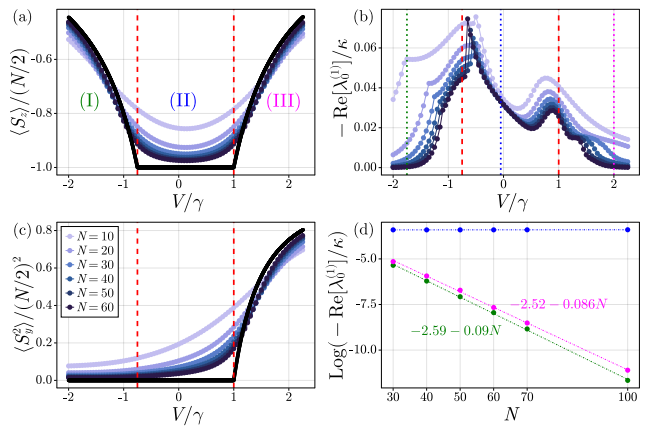


FIG. 3. Signatures of the 2nd-order DPT of the second model obtained from $\mathcal{L}_{\text{HEOM}}$, showing the emergence of three phases [(I), (II), and (III)] as V/γ is varied. (a) and (c): Steady-state values of $\langle S_z \rangle$ and $\langle S_y^2 \rangle$ as a function of V/γ for different N , allowing for distinguishing the phases. The solid black lines correspond to mean-field predictions and the vertical dashed red lines indicate the critical points. (b): Real part of $\lambda_0^{(1)}$ (i.e., the gap) as a function of V/γ , signalling the SSBs associated with the DPT. Three vertical dotted lines indicate the values of V/γ taken for the finite-size scaling of the gap shown in panel (d), i.e., $V/\gamma = -1.75$ (green), -0.05 (blue), 2 (pink), revealing an exponential closure of the gap in phases (I) and (III), as shown by the straight line fits. Parameters: $\omega = \kappa = 2h = 2\gamma$. Truncation orders: $k_{\text{max}} = 6$ ($N = 10-30$), 7 ($N = 40-60$), 9 ($N = 70, 100$).

and the vanishing of the gap, a task for which all other methods have failed so far (see SM).

Conclusion. We developed a comprehensive framework for studying DPTs in non-Markovian systems, more relevant experimentally. Our method is numerically exact, systematic, easily accessible (as based on the well-established HEOM technique available in open access libraries [25, 26]), and provides a considerable computational advantage over a standard embedding technique. We demonstrated the power of our approach by highlighting non-Markovian reservoir engineering of a 1st-order DPT with a discrete SSB, by showing how DPTs can be genuinely triggered by non-Markovian effects, and by capturing all the defining features of a challenging 2nd-order DPT with a continuous SSB for which other previous reduced descriptions had failed up to now [20].

Our work makes it possible to explore out-of-equilibrium matter phases beyond the idealized Markovian limit, featuring non-Markovianity as a resource for triggering or controlling them. This is so far uncharted territory as most works dealing with dissipative many-body dynamics is generally constrained to Lindblad dissipation, which potentially hinders the evidences of DPTs [19, 20]. Our method could be improved via hybridization with advanced numerical techniques, such as corner-space renormalization [59] or matrix product

operators (as in [51, 60–63]). Other perspectives include studies of initial system-bath correlations [64] or connections in the non-Markovian regime between DPTs and symmetry breaking [65, 66], geometric phase curvature [67, 68], or dynamical [69, 70] or measurement-induced [71, 72] phase transitions, or dissipation engineering of long-range order [73], also for systems with non-Lorentzian environments [28, 64, 74].

We thank Jonathan Keeling, Peter Kirton, Valentin Link and Lukas Pausch for helpful comments on a previous version of the manuscript. Computational resources were provided by the Consortium des Equipements de Calcul Intensif (CECI), funded by the Fonds de la Recherche Scientifique de Belgique (F.R.S.-FNRS) under Grant No. 2.5020.11.

-
- [1] J. Toner and Y. Tu, *Phys. Rev. E* **58**, 4828 (1998).
- [2] J. Jin, A. Biella, O. Viyuela, L. Mazza, J. Keeling, R. Fazio, and D. Rossini, *Phys. Rev. X* **6**, 031011 (2016).
- [3] T. E. Lee, S. Gopalakrishnan, and M. D. Lukin, *Phys. Rev. Lett.* **110**, 257204 (2013).
- [4] K. Baumann, C. Guerlin, F. Brennecke, and T. Esslinger, *Nature* **464**, 1301 (2010).
- [5] J. Klinder, H. Keßler, M. Wolke, L. Mathey, and A. Hemmerich, *Proceedings of the National Academy of Sciences* **112**, 3290 (2015), <https://www.pnas.org/doi/pdf/10.1073/pnas.1417132112>.
- [6] M. Fitzpatrick, N. M. Sundaresan, A. C. Y. Li, J. Koch, and A. A. Houck, *Phys. Rev. X* **7**, 011016 (2017).
- [7] J. M. Fink, A. Dombi, A. Vukics, A. Wallraff, and P. Domokos, *Phys. Rev. X* **7**, 011012 (2017).
- [8] T. Fink, A. Schade, S. Höfling, C. Schneider, and A. Imamoglu, *Nature Physics* **14**, 365–369 (2017).
- [9] J. Benary, C. Baals, E. Bernhart, J. Jiang, M. Röhrle, and H. Ott, *New Journal of Physics* **24**, 103034 (2022).
- [10] F. Minganti, A. Biella, N. Bartolo, and C. Ciuti, *Phys. Rev. A* **98**, 042118 (2018).
- [11] E. M. Kessler, G. Giedke, A. Imamoglu, S. F. Yelin, M. D. Lukin, and J. I. Cirac, *Phys. Rev. A* **86**, 012116 (2012).
- [12] M.-J. Hwang, P. Rabl, and M. B. Plenio, *Phys. Rev. A* **97**, 013825 (2018).
- [13] I. de Vega and D. Alonso, *Rev. Mod. Phys.* **89**, 015001 (2017).
- [14] S. F. Huelga, A. Rivas, and M. B. Plenio, *Phys. Rev. Lett.* **108**, 160402 (2012).
- [15] C. Maier, T. Brydges, P. Jurcevic, N. Trautmann, C. Hempel, B. P. Lanyon, P. Hauke, R. Blatt, and C. F. Roos, *Phys. Rev. Lett.* **122**, 050501 (2019).
- [16] V. Link, K. Müller, R. G. Lena, K. Luoma, F. Damanet, W. T. Strunz, and A. J. Daley, *PRX Quantum* **3**, 020348 (2022).
- [17] P. Chen, N. Yang, A. Couvertier, Q. Ding, R. Chatterjee, and T. Yu, *Chaos and entanglement in non-markovian optomechanical systems* (2023).
- [18] F. Otterpohl, P. Nalbach, and M. Thorwart, *Phys. Rev. Lett.* **129**, 120406 (2022).
- [19] F. Damanet, A. J. Daley, and J. Keeling, *Phys. Rev. A* **99**, 033845 (2019).
- [20] R. Palacino and J. Keeling, *Phys. Rev. Research* **3**, L032016 (2021).
- [21] Y. Tanimura and R. Kubo, *Journal of the Physical Society of Japan* **58**, 1199 (1989).
- [22] A. Ishizaki and Y. Tanimura, *Journal of the Physical Society of Japan* **74**, 3131 (2005), <https://doi.org/10.1143/JPSJ.74.3131>.
- [23] A. Ishizaki and G. R. Fleming, *Proceedings of the National Academy of Sciences* **106**, 17255 (2009), <https://www.pnas.org/doi/pdf/10.1073/pnas.0908989106>.
- [24] Y. Tanimura, *The Journal of Chemical Physics* **153**, 020901 (2020), <https://doi.org/10.1063/5.0011599>.
- [25] N. Lambert, T. Raheja, S. Cross, P. Menczel, S. Ahmed, A. Pitchford, D. Burgarth, and F. Nori, *Phys. Rev. Res.* **5**, 013181 (2023).
- [26] Y.-T. Huang, P.-C. Kuo, N. Lambert, M. Cirio, S. Cross, S.-L. Yang, F. Nori, and Y.-N. Chen, *arXiv preprint arXiv:2306.07522* (2023).
- [27] D. Nagy and P. Domokos, *Phys. Rev. Lett.* **115**, 043601 (2015).
- [28] D. Nagy and P. Domokos, *Phys. Rev. A* **94**, 063862 (2016).
- [29] P. Haikka, J. Gould, S. McEndoo, F. Plastina, and S. Maniscalco, *Phys. Rev. A* **85**, 060101(R) (2012).
- [30] A. Strathearn, P. Kirton, D. Kilda, J. Keeling, and B. Lovett, *Nature Communications* **9** (2018).
- [31] F. B. Anders, R. Bulla, and M. Vojta, *Phys. Rev. Lett.* **98**, 210402 (2007).
- [32] A. W. Chin, J. Prior, S. F. Huelga, and M. B. Plenio, *Phys. Rev. Lett.* **107**, 160601 (2011).
- [33] S. Florens, D. Venturelli, and R. Narayanan, *Quantum phase transition in the spin boson model*, in *Quantum Quenching, Annealing and Computation*, edited by A. K. Chandra, A. Das, and B. K. Chakrabarti (Springer Berlin Heidelberg, Berlin, Heidelberg, 2010) pp. 145–162.
- [34] T. E. Lee, C.-K. Chan, and S. F. Yelin, *Phys. Rev. A* **90**, 052109 (2014).
- [35] It should be noted that the formalism presented here is easily generalizable to multiple bosonic or fermionic baths at finite temperature.
- [36] Z. Tang, X. Ouyang, Z. Gong, H. Wang, and J. Wu, *The Journal of Chemical Physics* **143**, 224112 (2015), https://pubs.aip.org/aip/jcp/article-pdf/doi/10.1063/1.4936924/15506380/224112_1_online.pdf.
- [37] C. Meier and D. J. Tannor, *The Journal of Chemical Physics* **111**, 3365 (1999), <https://doi.org/10.1063/1.479669>.
- [38] G. Ritschel and A. Eisfeld, *The Journal of Chemical Physics* **141**, 094101 (2014), <https://doi.org/10.1063/1.4893931>.
- [39] R. Hartmann, M. Werther, F. Grossmann, and W. T. Strunz, *The Journal of Chemical Physics* **150**, 234105 (2019), <https://doi.org/10.1063/1.5097158>.
- [40] A. Imamoglu, *Phys. Rev. A* **50**, 3650 (1994).
- [41] B. J. Dalton, S. M. Barnett, and B. M. Garraway, *Phys. Rev. A* **64**, 053813 (2001).
- [42] B. M. Garraway, *Phys. Rev. A* **55**, 2290 (1997).
- [43] G. Pleasance, B. M. Garraway, and F. Petruccione, *Phys. Rev. Research* **2**, 043058 (2020).
- [44] L. Mazzola, S. Maniscalco, J. Piilo, K.-A. Suominen, and B. M. Garraway, *Phys. Rev. A* **80**, 012104 (2009).
- [45] H. Yang, H. Miao, and Y. Chen, *Phys. Rev. A* **85**, 040101(R) (2012).
- [46] H.-P. Breuer, *Phys. Rev. A* **70**, 012106 (2004).

- [47] A. Barchielli, C. Pellegrini, and F. Petruccione, *EPL (Europhysics Letters)* **91**, 24001 (2010).
- [48] S. Schmidt and J. Koch, *Ann. Phys.* **525**, 395 (2013).
- [49] A. Blais, A. L. Grimsmo, S. M. Girvin, and A. Wallraff, *Rev. Mod. Phys.* **93**, 025005 (2021).
- [50] S. Flannigan, F. Damanet, and A. J. Daley, *Phys. Rev. Lett.* **128**, 063601 (2022).
- [51] M. Moroder, M. Grundner, F. Damanet, U. Schollwöck, S. Mardazad, S. Flannigan, T. Köhler, and S. Paeckel, *Phys. Rev. B* **107**, 214310 (2023).
- [52] K. Santhosh, O. Bitton, L. Chuntonov, and G. Haran, *Nature Communications* **7** (2015).
- [53] F. Mascherpa, A. Smirne, A. D. Somoza, P. Fernández-Acebal, S. Donadi, D. Tamascelli, S. F. Huelga, and M. B. Plenio, *Phys. Rev. A* **101**, 052108 (2020).
- [54] C. Duan, Z. Tang, J. Cao, and J. Wu, *Phys. Rev. B* **95**, 214308 (2017).
- [55] Indeed, by definition of the steady-state, we have $\mathcal{L}_{\text{HEOM}}|\rho_{ss}\rangle\rangle = 0$, from which we get $\mathcal{U}\mathcal{L}_{\text{HEOM}}|\rho_{ss}\rangle\rangle = \mathcal{L}_{\text{HEOM}}\mathcal{U}|\rho_{ss}\rangle\rangle = 0$ by definition of the symmetry. Since $|\rho_{ss}\rangle\rangle$ is unique, we must have $\mathcal{U}|\rho_{ss}\rangle\rangle = |\rho_{ss}\rangle\rangle$, which shows that $|\rho_{ss}\rangle\rangle \in L_{u=1}$.
- [56] F. Minganti, V. Savona, and A. Biella, *Dissipative phase transitions in n -photon driven quantum nonlinear resonators* (2023), arXiv:2303.03355 [quant-ph].
- [57] S. Morrison and A. S. Parkins, *Phys. Rev. A* **77**, 043810 (2008).
- [58] R. I. Moodie, K. E. Ballantine, and J. Keeling, *Phys. Rev. A* **97**, 033802 (2018).
- [59] S. Finazzi, A. Le Boité, F. Storme, A. Baksic, and C. Ciuti, *Phys. Rev. Lett.* **115**, 080604 (2015).
- [60] E. Mascarenhas, H. Flayac, and V. Savona, *Phys. Rev. A* **92**, 022116 (2015).
- [61] J. Cui, J. I. Cirac, and M. C. Bañuls, *Phys. Rev. Lett.* **114**, 220601 (2015).
- [62] S. Flannigan, F. Damanet, and A. J. Daley, arXiv (2021).
- [63] V. Link, H.-H. Tu, and W. T. Strunz, *Open quantum system dynamics from infinite tensor network contraction* (2023), arXiv:2307.01802 [quant-ph].
- [64] T. Ikeda and G. D. Scholes, *The Journal of Chemical Physics* **152**, 10.1063/5.0007327 (2020).
- [65] J. Huber, P. Kirton, and P. Rabl, *Phys. Rev. A* **102**, 012219 (2020).
- [66] F. Minganti, I. I. Arkhipov, A. Miranowicz, and F. Nori, *New Journal of Physics* **23**, 122001 (2021).
- [67] A. Carollo, D. Valenti, and B. Spagnolo, *Physics Reports* **838**, 1 (2020), geometry of quantum phase transitions.
- [68] A. Carollo, B. Spagnolo, and D. Valenti, *Scientific Reports* **8** (2018).
- [69] T. H. Kyaw, V. M. Bastidas, J. Tangpanitanon, G. Romero, and L.-C. Kwek, *Phys. Rev. A* **101**, 012111 (2020).
- [70] D. Dolgitzer, D. Zeng, and Y. Chen, *Opt. Express* **29**, 23988 (2021).
- [71] M. Buchhold, Y. Minoguchi, A. Altland, and S. Diehl, *Phys. Rev. X* **11**, 041004 (2021).
- [72] T. Müller, S. Diehl, and M. Buchhold, *Phys. Rev. Lett.* **128**, 010605 (2022).
- [73] J. Tindall, B. Buča, J. R. Coulthard, and D. Jaksch, *Phys. Rev. Lett.* **123**, 030603 (2019).
- [74] R. Lundgren, A. V. Gorshkov, and M. F. Maghrebi, *Phys. Rev. A* **102**, 032218 (2020).

Supplemental Material: Spectral Theory of Non-Markovian Dissipative Phase Transitions

Baptiste Debecker, John Martin, François Damanet
*Institut de Physique Nucléaire, Atomique et de Spectroscopie,
CESAM, University of Liège, B-4000 Liège, Belgium*

This Supplemental Material provides analytical and numerical details on the results presented in the main text of “Spectral Theory of Non-Markovian Dissipative Phase Transitions”. In Sec. I, we provide an example of explicit constructions of the HEOM’s Liouvillian $\mathcal{L}_{\text{HEOM}}$. In Sec. II, we give a general argument on the computational advantage of using $\mathcal{L}_{\text{HEOM}}$ over the standard Markovian embedding technique illustrated in Fig. 1 of the main text. In Sec. III, we give the proofs of the properties of $\mathcal{L}_{\text{HEOM}}$ stated in the main text, as well as their connections to DPTs. In Sec. IV and V, we provide details on the 1st-order DPT in the Lipkin-Meshkov-Glick model and on the 2nd-order DPTs in the extended one investigated in the main text. In Sec. VI, we present the case of a third model, i.e., a two-mode Dicke model with a continuous symmetry. Finally, in Sec. VII, we present convergence analyses of our method for the first and third models we consider, which we compare with the enlarged Markovian system technique.

CONTENTS

I. Explicit matrix form of the HEOM’s Liouvillian	2
II. Computational advantage of $\mathcal{L}_{\text{HEOM}}$ - General argument	2
III. Properties of the HEOM Liouvillian and connections to DPTs	3
A. Remark on notations	3
B. Proof of the properties of the HEOM Liouvillian	3
C. Connections to DPTs	4
1. 1 st -order DPTs	4
2. 2 nd -order DPTs with SSB	7
IV. First model - Shifting phase boundaries via non-Markovian effects	8
A. Adiabatic elimination of the cavity mode in the bad cavity limit	8
B. Mean-field analysis	9
1. Spin model	11
2. Full model	12
C. Understanding the emergence of 1 st -order DPTs with spectral decompositions	14
D. Impact of non-Markovianity on the critical point	15
V. Second model - Triggering DPTs via non-Markovian effects	15
A. Mean-field analysis	16
B. Understanding the emergence of 2 nd -order DPT from spectral decompositions	17
VI. Third model - Challenging two-mode Dicke model	17
VII. Convergence analysis and numerical efficiency	18
A. Convergence analysis of $\mathcal{L}_{\text{HEOM}}(k_{\text{max}})$	18
B. Comparison with enlarged Markovian systems	21
References	21

I. EXPLICIT MATRIX FORM OF THE HEOM'S LIOUVILLIAN

By vectorizing Eq. (3) of the main text using $|i\rangle\langle j| \cong |i\rangle \otimes |j\rangle$ [S1], we get

$$\begin{aligned} \frac{d|\rho^{(\vec{n}, \vec{m})}\rangle\rangle}{dt} = & -i [H_S \otimes \mathbf{1} - \mathbf{1} \otimes H_S^T - (\vec{w}^* \cdot \vec{n} + \vec{w} \cdot \vec{m})] |\rho^{(\vec{n}, \vec{m})}\rangle\rangle + \sum_{j=1}^M \left(G_j n_j L_j \otimes \mathbf{1} |\rho^{(\vec{n}-\vec{e}_j, \vec{m})}\rangle\rangle \right. \\ & \left. + G_j^* m_j \mathbf{1} \otimes L_j^* |\rho^{(\vec{n}, \vec{m}-\vec{e}_j)}\rangle\rangle \right) + \sum_{j=1}^M \left[(\mathbf{1} \otimes L_j^* - L_j^\dagger \otimes \mathbf{1}) |\rho^{(\vec{n}+\vec{e}_j, \vec{m})}\rangle\rangle (\mathbf{1} \otimes L_j^* - L_j^\dagger \otimes \mathbf{1})^\dagger |\rho^{(\vec{n}, \vec{m}+\vec{e}_j)}\rangle\rangle \right], \quad (\text{S1}) \end{aligned}$$

where $|\rho^{(\vec{n}, \vec{m})}\rangle\rangle$ denotes the vectorization of the matrices $\rho^{(\vec{n}, \vec{m})}$, $\mathbf{1}$ the identity matrix acting on \mathcal{H}_S , and L_j^* (L_j^T) the conjugate (transpose) matrix of L_j . By stacking in a vector $|\rho\rangle\rangle$ all the vectorized matrices $|\rho^{(\vec{n}, \vec{m})}\rangle\rangle$, we can construct the matrix $\mathcal{L}_{\text{HEOM}}(k_{\text{max}})$ called *HEOM's Liouvillian* and Eq. (S1) becomes Eq. (4) of the main text, i.e.,

$$\frac{d|\rho\rangle\rangle}{dt} = \mathcal{L}_{\text{HEOM}}(k_{\text{max}}) |\rho\rangle\rangle. \quad (\text{S2})$$

For the sake of clarity, we explicitly construct the different blocks of the matrix representation of the HEOM's Liouvillian for an environment made of only one damped pseudo-mode ($M = 1$). For this special case, the vectorized HEOM reads

$$\begin{aligned} \frac{d|\rho^{(n,m)}\rangle\rangle}{dt} = & \underbrace{[-i (H_S \otimes \mathbf{1} - \mathbf{1} \otimes H_S^T) - ((n-m)i\omega + (n+m)\kappa) \mathbf{1} \otimes \mathbf{1}]}_{\equiv D_{nm}} |\rho^{(n,m)}\rangle\rangle \\ & + \underbrace{(Gn L \otimes \mathbf{1})}_{\equiv A_n} |\rho^{(n-1,m)}\rangle\rangle + \underbrace{(G^* m \mathbf{1} \otimes L^*)}_{\equiv B_m} |\rho^{(n,m-1)}\rangle\rangle \\ & + \underbrace{(\mathbf{1} \otimes L^* - L^\dagger \otimes \mathbf{1})}_{\equiv C} |\rho^{(n+1,m)}\rangle\rangle + \underbrace{(L \otimes \mathbf{1} - \mathbf{1} \otimes L^T)}_{\equiv -C^\dagger} |\rho^{(n,m+1)}\rangle\rangle. \end{aligned}$$

Therefore, if $k_{\text{max}} = 1$, the stacked vector $|\rho\rangle\rangle$ is given by $|\rho\rangle\rangle = (|\rho^{(0,0)}\rangle\rangle, |\rho^{(0,1)}\rangle\rangle, |\rho^{(1,0)}\rangle\rangle)^T$ and

$$\mathcal{L}_{\text{HEOM}}(k_{\text{max}} = 1) = \begin{pmatrix} D_{00} & -C^\dagger & C \\ B_1 & D_{01} & 0 \\ A_1 & 0 & D_{10} \end{pmatrix}, \quad (\text{S3})$$

while for $k_{\text{max}} = 2$, we get $|\rho\rangle\rangle = (|\rho^{(0,0)}\rangle\rangle, |\rho^{(0,1)}\rangle\rangle, |\rho^{(0,2)}\rangle\rangle, |\rho^{(1,0)}\rangle\rangle, |\rho^{(1,1)}\rangle\rangle, |\rho^{(2,0)}\rangle\rangle)^T$ and

$$\mathcal{L}_{\text{HEOM}}(k_{\text{max}} = 2) = \begin{pmatrix} D_{00} & -C^\dagger & 0 & C & 0 & 0 \\ B_1 & D_{01} & -C^\dagger & 0 & C & 0 \\ 0 & B_2 & D_{02} & 0 & 0 & 0 \\ A_1 & 0 & 0 & D_{10} & -C^\dagger & C \\ 0 & A_1 & 0 & B_1 & D_{11} & 0 \\ 0 & 0 & 0 & A_2 & 0 & D_{20} \end{pmatrix}. \quad (\text{S4})$$

II. COMPUTATIONAL ADVANTAGE OF $\mathcal{L}_{\text{HEOM}}$ - GENERAL ARGUMENT

In this section, we compare the dimension of the HEOM Liouvillian $\mathcal{L}_{\text{HEOM}}$ to the one of the Liouvillian for the enlarged Markovian system that includes the pseudomodes, which we denote by \mathcal{L}_M . This provides an overall idea of what kind of computational advantage of using $\mathcal{L}_{\text{HEOM}}$ instead of \mathcal{L}_M can be expected. A more detailed comparison for the LMG model investigated in the main text can be found in Sec. V.

The dimension of the matrix representing $\mathcal{L}_{\text{HEOM}}$ is

$$D = \dim(\mathcal{L}_{\text{HEOM}}) = \frac{(2M + k_{\text{max}})!}{(2M)!k_{\text{max}}!} \dim(\mathcal{H}_S)^2 \quad (\text{S5})$$

It depends on the size of the system Hilbert space \mathcal{H}_S , and of the truncation order k_{max} and the number of pseudo modes M which determines the number of auxiliary matrices of the hierarchy.

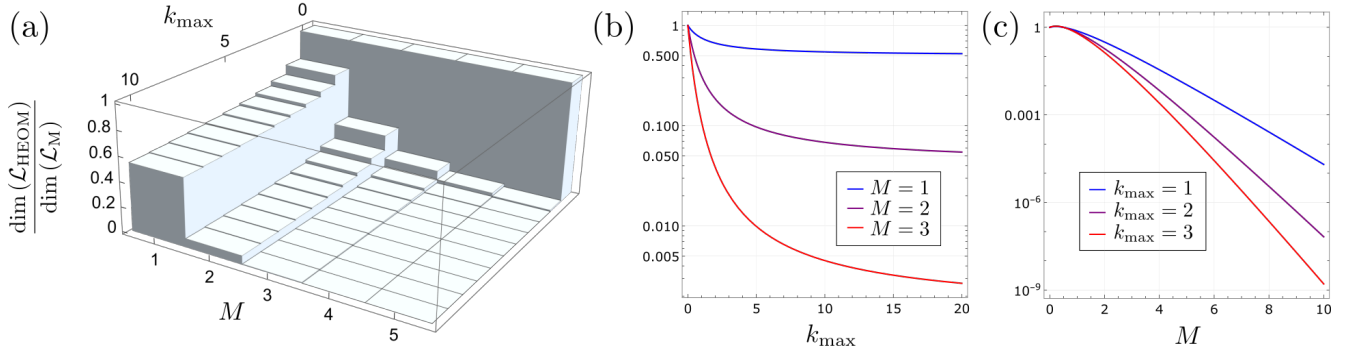


FIG. S1. Overall comparison between the dimensions of $\mathcal{L}_{\text{HEOM}}$ and \mathcal{L}_M : ratios $\dim(\mathcal{L}_{\text{HEOM}})/\dim(\mathcal{L}_M)$ as a function k_{max} and M (a), as a function of k_{max} for $M = 1, 2$ and 3 (b), and as a function of M for $k_{\text{max}} = 1, 2$ and 3 (c). Since $\dim(\mathcal{L}_{\text{HEOM}})/\dim(\mathcal{L}_M) < 1$, this means that we need less computational memory to store $\mathcal{L}_{\text{HEOM}}$ than \mathcal{L}_M .

To compare with the dimension of the matrix representing the Liouvillian of the enlarged Markovian system \mathcal{L}_M , we need to introduce a cutoff N_c for the pseudo-mode Fock spaces $\{|n_i\rangle\}$ ($n_i = 0, 1, \dots, \infty$ and $i = 1, 2, \dots, M$), which are in principle infinite. We choose here $N_c = k_{\text{max}}$, motivated by the fact that the pseudo-mode correlation functions are related to the traces of the auxiliary matrices according to (for $M = 1$) [S2]

$$\langle a^n (a^\dagger)^m \rangle(t) = \frac{\text{Tr}[\rho^{(n,m)}(t)]}{(iG)^n (-iG)^m}, \quad (\text{S6})$$

which means that if we truncate the hierarchy at k_{max} , we need at least to truncate the pseudo-mode Fock space at $N_c = k_{\text{max}}$ to be able to compute the same correlations. The dimension of \mathcal{L}_M should thus be

$$\dim(\mathcal{L}_M) = \dim(\mathcal{H}_S)^2 (k_{\text{max}} + 1)^M. \quad (\text{S7})$$

The ratio $\dim(\mathcal{L}_{\text{HEOM}})/\dim(\mathcal{L}_M)$ is plotted as a function of k_{max} and M in Fig. S1. We see that the advantage can be significant, especially for large numbers of pseudo-modes.

III. PROPERTIES OF THE HEOM LIOUVILLIAN AND CONNECTIONS TO DPTS

A. Remark on notations

$\mathcal{L}_{\text{HEOM}}(k_{\text{max}})$ is a superoperator, which can be represented in the finite dimensional case by a matrix thanks to the Choi-Jamiolkowski isomorphism, as explained in the main text and in Section I. For simplicity and clarity, we choose to not change the notations when $\mathcal{L}_{\text{HEOM}}$ is seen as a superoperator or as a matrix. Instead, it is the object it acts on that changes, i.e., $\rho = \{\rho^{(\vec{n}, \vec{m})} | \sum_j (n_j + m_j) \leq k_{\text{max}}\}$ or $|\rho\rangle\rangle = \{|\rho^{(\vec{n}, \vec{m})}\rangle\rangle | \sum_j (n_j + m_j) \leq k_{\text{max}}\}$, so that no ambiguity should arise. As an illustration, for one damped pseudo-mode ($M = 1$), $k_{\text{max}} = 1$, and $L_j \equiv L$, we have that

$$\mathcal{L}_{\text{HEOM}}(k_{\text{max}} = 1)|\rho\rangle\rangle = \begin{pmatrix} D_{00} & -C^\dagger & C \\ B_1 & D_{01} & 0 \\ A_1 & 0 & D_{10} \end{pmatrix} \begin{pmatrix} |\rho^{(0,0)}\rangle\rangle \\ |\rho^{(0,1)}\rangle\rangle \\ |\rho^{(1,0)}\rangle\rangle \end{pmatrix}, \quad (\text{S8})$$

$$\mathcal{L}_{\text{HEOM}}(k_{\text{max}} = 1)[\rho] = \begin{pmatrix} \frac{d}{dt}\rho^{(0,0)} \\ \frac{d}{dt}\rho^{(0,1)} \\ \frac{d}{dt}\rho^{(1,0)} \end{pmatrix} = \begin{pmatrix} -i[H_S, \rho^{(0,0)}] + [\rho^{(1,0)}, L^\dagger] + [L, \rho^{(0,1)}] \\ -i[H_S, \rho^{(0,1)}] + (i\omega - \kappa)\rho^{(0,1)} + G^* \rho^{(0,0)} L^\dagger \\ -i[H_S, \rho^{(1,0)}] - (i\omega + \kappa)\rho^{(1,0)} + GL\rho^{(0,0)} \end{pmatrix},$$

where we used in the first line the notations of Section I.

B. Proof of the properties of the HEOM Liouvillian

We provide here the proofs of the properties of the HEOM Liouvillian. To show that the spectrum of $\mathcal{L}_{\text{HEOM}}$ is symmetric with respect to the real axis (property (i) of the main text), we note that $\left(\frac{d\rho^{(\vec{n}, \vec{m})}}{dt}\right)^\dagger = \frac{d}{dt}\rho^{(\vec{m}, \vec{n})} =$

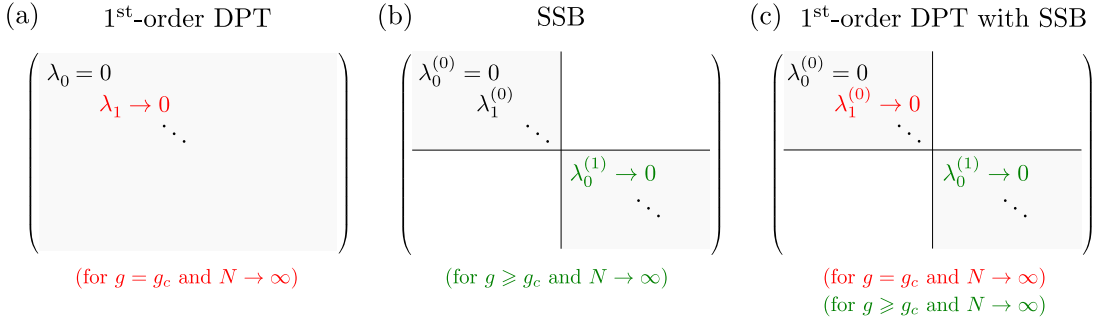


FIG. S2. Main properties of the behavior of key eigenvalues of the HEOM Liouvillian in the thermodynamic limit $N \rightarrow \infty$ in different scenarii. (a) When there is a 1st-order DPT, the first non-zero eigenvalue λ_1 should vanish at the critical point. (b) When the Liouvillian can be decomposed in symmetry sectors (illustrated here for the case of two symmetry sectors $k = 0$ and $k = 1$) and there is a SSB, the first non-zero eigenvalue of the Liouvillian in each symmetry sector different from the one of the steady state (i.e., $\lambda_0^{(k)}$ for $k > 0$) should vanish in the symmetry broken phase ($g \geq g_c$). (c) When there is both a 1st-order DPT and a SSB, the system exhibits the combined behavior of cases (a) and (b), where the eigenvalue vanishing only at g_c is the one in the symmetry sector of the steady state (i.e., $\lambda_1^{(0)}$).

$\frac{d}{dt}(\rho^{(\vec{n}, \vec{m})})^\dagger$, where we used the property $(\rho^{(\vec{n}, \vec{m})})^\dagger = \rho^{(\vec{m}, \vec{n})}$ [S2], which implies

$$\mathcal{L}_{\text{HEOM}}[\rho^\dagger] = (\mathcal{L}_{\text{HEOM}}[\rho])^\dagger. \quad (\text{S9})$$

The trace preserving property ((ii) in the main text) of $\mathcal{L}_{\text{HEOM}}$ is immediate from Eq. (3) of the main text. This implies that

$$0 = \frac{d\text{Tr}[\rho^{(\vec{0}, \vec{0})}]}{dt} = \text{Tr} \left[\frac{d}{dt} \rho^{(\vec{0}, \vec{0})} \right] = \text{Tr} \left[\mathbb{1}^{(\vec{0}, \vec{0})} \mathcal{L}_{\text{HEOM}}[\rho] \right] = \langle \langle \mathbb{1}^{(\vec{0}, \vec{0})} | \mathcal{L}_{\text{HEOM}}[\rho] \rangle \rangle \quad \forall \rho, \quad (\text{S10})$$

where we used the Hilbert-Schmidt inner product $\langle \langle A|B \rangle \rangle \equiv \text{Tr}[A^\dagger B]$ and the projector onto the physical state space $\mathbb{1}^{(\vec{0}, \vec{0})}$. Equation (S10) leads to $\langle \langle \mathbb{1}^{(\vec{0}, \vec{0})} | \mathcal{L}_{\text{HEOM}} = 0$, meaning that $\langle \langle \mathbb{1}^{(\vec{0}, \vec{0})} |$ is a left eigenvector of $\mathcal{L}_{\text{HEOM}}$ associated to the eigenvalue 0. Therefore, the eigenvalue 0 is always in the spectrum of $\mathcal{L}_{\text{HEOM}}$ (property (iii) of the main text), which guarantees the existence of a stationary state. The fact that all the eigenvalues must have a negative real part in the limit $k_{\text{max}} \rightarrow +\infty$ (property (iv) of the main text) comes from the fact that in this limit, the solution of Eq. (3) of the main text in the sector $(\vec{0}, \vec{0})$ is *exactly* the reduced density operator of the system. Thus, any positive real part eigenvalues would lead to unphysical matrices in the sector $(\vec{0}, \vec{0})$, therefore contradicting our last statement. Lastly, to prove that $\text{Tr}[\mathbb{1}^{(\vec{0}, \vec{0})} \rho_i] = 0$ if ρ_i is a right eigenoperator of $\mathcal{L}_{\text{HEOM}}$ associated to the eigenvalue λ_i with $\text{Re}[\lambda_i] \neq 0$ (property (v) of the main text), we note that $\mathcal{L}_{\text{HEOM}}$ preserves the trace in the sector $(\vec{0}, \vec{0})$ and $\rho_i(t) = e^{\mathcal{L}_{\text{HEOM}} t} \rho_i \rightarrow 0$ for $t \rightarrow +\infty$ if $\text{Re}[\lambda_i] \neq 0$ and $k_{\text{max}} \rightarrow +\infty$.

C. Connections to DPTs

In this section, we discuss how the properties of the HEOM Liouvillian are connected to 1st-order DPTs and to 2nd-order DPTs associated with spontaneous symmetry breaking (SSB). A summary of the behavior of the key eigenvalues of the HEOM Liouvillian for the different cases can be seen in Fig. (S2).

1. 1st-order DPTs

Since 1st-order DPTs are independent of symmetries of the HEOM Liouvillian $\mathcal{L}_{\text{HEOM}}$ (and thus of SSB), we consider below no particular symmetry and simply label the eigenvectors and eigenvalues of $\mathcal{L}_{\text{HEOM}}$ as ρ_i and λ_i . In the case of 1st-order DPTs emerging in systems with symmetries, the results below must be understood as related to the Liouvillian block associated with the symmetry sector containing the steady state, i.e., the block $\mathcal{L}_{u_0=1}$ of the decomposition $\mathcal{L}_{\text{HEOM}} = \bigoplus_{u_k} \mathcal{L}_{u_k}$, so that ρ_i and λ_i below must simply be understood as $\rho_i^{(0)}$ and $\lambda_i^{(0)}$. This is exemplified in Fig. 2 of the main text, where we show both the eigenvalue signalling the SSB ($\lambda_0^{(1)}$) and the one responsible for the 1st-order DPT ($\lambda_1^{(0)}$).

Because of the aforementioned properties and their similarity with the Markovian case [S3], one can show that a 1st-order DPT can occur if and only if the HEOM Liouvillian gap $\text{Re}[\lambda_1]$ vanishes at the critical point in the thermodynamic limit. Moreover, $\text{Im}[\lambda_1]$ must vanish in a finite domain around the critical point. For the sake of completeness, we prove below these statements in the limit $k_{\text{max}} \rightarrow +\infty$. The proofs closely follow Ref. [S3] which itself relies on results of Kato [S4]. We start by a definition.

Definition III.1. Let ρ_i be a right eigenoperator of $\mathcal{L}_{\text{HEOM}}$. We define the superoperator $\mathcal{P}^{(\vec{0}, \vec{0})}$ through

$$\mathcal{P}^{(\vec{0}, \vec{0})} \rho_i = \rho_i^{(\vec{0}, \vec{0})}, \quad |\mathcal{P}^{(\vec{0}, \vec{0})} \rho_i\rangle = |\rho_i^{(\vec{0}, \vec{0})}\rangle, \quad (\text{S11})$$

i.e., $\mathcal{P}^{(\vec{0}, \vec{0})}$ only selects the component of ρ_i in the physical sector $(\vec{0}, \vec{0})$, that is the operator $\rho_i^{(\vec{0}, \vec{0})}$ acting on a space of dimension $\dim(\mathcal{H}_S)$. Note that $\mathcal{P}^{(\vec{0}, \vec{0})}$ is different from $\mathbb{1}^{(\vec{0}, \vec{0})}$, as $|\mathbb{1}^{(\vec{0}, \vec{0})} \rho_i\rangle$ corresponds to the stacked vector $(|\rho_i^{(\vec{0}, \vec{0})}\rangle, |0\rangle, |0\rangle, \dots)^T$.

Proposition III.1. *If a physical system undergoes a 1st-order DPT in a well-defined thermodynamic limit $N \rightarrow +\infty$ at the critical point $g = g_c$ separating two unique phases, and if $\lim_{N \rightarrow +\infty} \mathcal{L}_{\text{HEOM}}(g, N)$ is continuous with respect to g , then $\lim_{N \rightarrow +\infty} \lambda_1(g = g_c, N) = 0$.*

Proof. Let us assume that a system undergoes a 1st-order DPT in a well-defined thermodynamic limit $N \rightarrow +\infty$ when a parameter g is varied. By definition, the steady state $\rho^{(\vec{0}, \vec{0})}(t \rightarrow \infty) \equiv \rho_{ss}^{(\vec{0}, \vec{0})}$ must change discontinuously, which implies that there exists a critical point g_c such that

$$\lim_{g \rightarrow g_c^-} \lim_{N \rightarrow +\infty} \rho_{ss}^{(\vec{0}, \vec{0})}(g, N) \equiv \rho_-^{(\vec{0}, \vec{0})} \neq \lim_{g \rightarrow g_c^+} \lim_{N \rightarrow +\infty} \rho_{ss}^{(\vec{0}, \vec{0})}(g, N) \equiv \rho_+^{(\vec{0}, \vec{0})}, \quad (\text{S12})$$

where $\rho_-^{(\vec{0}, \vec{0})}$ and $\rho_+^{(\vec{0}, \vec{0})}$ are the states (phases) of the system right before and after the transition, respectively, which are unique by hypothesis. Equation (S12) implies that there exists ρ_{\pm} such that

$$\lim_{g \rightarrow g_c^-} \lim_{N \rightarrow +\infty} \mathcal{L}_{\text{HEOM}}(g, N)[\rho_-] = 0 = \lim_{g \rightarrow g_c^+} \lim_{N \rightarrow +\infty} \mathcal{L}_{\text{HEOM}}(g, N)[\rho_+], \quad (\text{S13})$$

with $\mathcal{P}^{(\vec{0}, \vec{0})} \rho_{\pm} = \rho_{\pm}^{(\vec{0}, \vec{0})}$. The continuity of the HEOM generator in the thermodynamic limit then gives

$$\lim_{g \rightarrow g_c} \lim_{N \rightarrow +\infty} \mathcal{L}_{\text{HEOM}}(g, N)[\rho_{\pm}] = 0. \quad (\text{S14})$$

Exactly at $g = g_c$, we then found two eigenoperators that belongs to the null space of $\mathcal{L}_{\text{HEOM}}$, while there is a unique steady state for $g \neq g_c$. Consequently, we must have

$$\lim_{N \rightarrow +\infty} \lambda_1(g = g_c, N) = 0 = \lambda_0, \quad \lim_{N \rightarrow +\infty} \lambda_1(g \neq g_c, N) \neq 0. \quad (\text{S15})$$

□

Note that even if $\mathcal{L}_{\text{HEOM}}(g)$ is continuous, there is no guarantee that $\rho_1(g)$ is continuous. Indeed, the coalescence of eigenvalues may induce non-continuous eigenvectors [S4]. Nevertheless, we will get rid of these difficulties by assuming that $\rho_1^{(\vec{0}, \vec{0})} \equiv \mathcal{P}^{(\vec{0}, \vec{0})} \rho_1$ is continuous, as done for the Markovian case [S3]. We can then elaborate on the form of the steady state at the critical point as a function of the right eigenvectors of the Liouvillian associated with λ_0 and λ_1 , that is ρ_0 and ρ_1 . For convenience, from now on we always assume the thermodynamic limit and drop the N dependence.

Proposition III.2. *We retain the same assumptions as in Proposition III.1. If ρ_+ and ρ_- span the null space at $g = g_c$, then $\text{Im}[\lambda_1] = 0$ holds in a finite neighborhood of $g = g_c$. Moreover, if $\lim_{N \rightarrow +\infty} \rho_1^{(\vec{0}, \vec{0})}(g, N)$ is continuous with respect to g and orthogonal to the steady-state, then*

$$\rho_{ss}^{(\vec{0}, \vec{0})}(g = g_c) = \frac{\rho_+^{(\vec{0}, \vec{0})} + \rho_-^{(\vec{0}, \vec{0})}}{2}, \quad (\text{S16})$$

in the thermodynamic limit, i.e., the steady-state is an equal mixture of the two phases ρ^{\pm} .

Proof. We must have $\text{Im}[\lambda_1] = 0$ in a finite neighbourhood of g_c as if it were not the case, then we would have three zero eigenvalues at $g = g_c$: $\lambda_1(g = g_c) = \lambda_1^*(g = g_c) = \lambda_0 = 0$ because of the property (i) of the main text. This implies that ρ^+ and ρ^- do not span the null space at $g = g_c$ ¹, which contradicts our assumptions.

To prove the second part, we first note that from the property (v) of $\mathcal{L}_{\text{HEOM}}$, we have $\text{Tr}[\mathbb{1}^{(\vec{0},\vec{0})}\rho_1(g \neq g_c)] = 0$ since $\text{Re}[\lambda_1(g \neq g_c)] \neq 0$. By hypothesis $\rho_1^{(\vec{0},\vec{0})} \equiv \mathcal{P}^{(\vec{0},\vec{0})}\rho_1$ is continuous. This means that $\rho_1^{(\vec{0},\vec{0})}(g)$ does not change abruptly as a function g but instead evolves continuously and makes a small excursion into the null space of $\mathcal{L}_{\text{HEOM}}$ exactly at $g = g_c$. Therefore, we extend the zero trace property of $\rho_1^{(\vec{0},\vec{0})}$ at the critical point. Since the system null space at $g = g_c$ is spanned by $\rho_{\pm}^{(\vec{0},\vec{0})}$, we must have

$$\rho_1^{(\vec{0},\vec{0})}(g = g_c) \propto \rho_+^{(\vec{0},\vec{0})} - \rho_-^{(\vec{0},\vec{0})}. \quad (\text{S17})$$

Furthermore, since $\rho_{\pm}^{(\vec{0},\vec{0})}$ span the null space at $g = g_c$, the steady state at the critical point must read

$$\rho_{ss}(g = g_c) = c\rho_+^{(\vec{0},\vec{0})} + (1 - c)\rho_-^{(\vec{0},\vec{0})}, \quad (\text{S18})$$

with $c \in [0, 1]$. The precise value of c cannot be determined through the behavior of $\rho_{ss}(g \neq g_c)$. If, however, we impose orthogonality between $\rho_{ss}(g = g_c)$ and $\rho_1^{(\vec{0},\vec{0})}(g = g_c)$, we obtain

$$\rho_{ss}^{(\vec{0},\vec{0})}(g = g_c) = \frac{\rho_+^{(\vec{0},\vec{0})} + \rho_-^{(\vec{0},\vec{0})}}{2}, \quad (\text{S19})$$

in virtue of the orthogonality between $\rho_{\pm}^{(\vec{0},\vec{0})}$, that we prove below.

For $\lambda_1(g = g_c) = 0 \in \mathbb{R}$, $\rho_1^{(\vec{0},\vec{0})}$ can be assumed Hermitian without loss of generality, as a direct consequence of property (i) of the main text. Consequently, $\rho_1^{(\vec{0},\vec{0})}$ can be diagonalized and one can construct ρ^{\pm} , satisfying Eq. (S17), by simply gathering all positive eigenvalues in $\rho_+^{(\vec{0},\vec{0})}$ and all negative eigenvalues in $-\rho_-^{(\vec{0},\vec{0})}$ and then normalizing the trace of $\rho_{\pm}^{(\vec{0},\vec{0})}$ to one. By construction, $\rho_{\pm}^{(\vec{0},\vec{0})}$ are then orthogonal. \square

We stress that the decomposition (S16) relies on strong assumptions, *e.g.*, the orthogonality of $\rho_1^{(\vec{0},\vec{0})}$ and ρ_{ss} at the critical point, which may not be fulfilled. Indeed, in Ref. [S5], it has been shown that, in the Markovian regime, there exists 1st-order DPTs without phase coexistence at the critical point, which contradicts Eq. (S16). Nevertheless, in all the systems studied here we find an excellent agreement with the present theory. Indeed, we numerically checked the validity of the decomposition (S16) and find good agreement as discussed in Section IV.C.

Proposition III.3. *If $\lambda_1(g)$ vanishes only at $g = g_c$ with $\text{Im}[\lambda_1(g)] = 0$ in a finite domain around $g = g_c$, $\rho_1^{(\vec{0},\vec{0})}(g)$ is continuous and if the null space is spanned at $g = g_c$ by two linearly independent eigenoperators associated with the eigenvalue 0, then there is a 1st-order DPT occurring at $g = g_c$.*

Proof. We proceed by contradiction by assuming that $\lim_{g \rightarrow g_c} \lambda_1(g) = 0$ and that there is no 1st-order DPT. Equivalently, we have that for any observable O of the system $\text{Tr}[O\rho_{ss}](g)$ is continuous at $g = g_c$, which implies that $\rho_{ss}^{(\vec{0},\vec{0})}(g)$ is also continuous at $g = g_c$. At $g = g_c$, however, $\lambda_1 = 0$ and as in Proposition III.2, we may then extend the zero trace condition by setting

$$\rho_1^{(\vec{0},\vec{0})}(g = g_c) \propto \rho_{1+}^{(\vec{0},\vec{0})} - \rho_{1-}^{(\vec{0},\vec{0})}, \quad (\text{S20})$$

where $\rho_{1\pm}^{(\vec{0},\vec{0})}$ can be found by diagonalizing $\rho_1^{(\vec{0},\vec{0})}$ [which is always possible since $\rho_1^{(\vec{0},\vec{0})}$ is hermitian in the domain in which $\text{Im}[\lambda_1] = 0$] and gathering again all positive eigenvalues in $\rho_{1+}^{(\vec{0},\vec{0})}$ and all negative eigenvalues in $-\rho_{1-}^{(\vec{0},\vec{0})}$ and then normalizing the trace of $\rho_{1\pm}^{(\vec{0},\vec{0})}$ to one. By construction, $\rho_{1\pm}^{(\vec{0},\vec{0})}$ are then density matrices such that $\langle\langle \rho_{1+}^{(\vec{0},\vec{0})} | \rho_{1-}^{(\vec{0},\vec{0})} \rangle\rangle \equiv \text{Tr}[\rho_{1+}^{(\vec{0},\vec{0})\dagger} \rho_{1-}^{(\vec{0},\vec{0})}] = 0$. At the critical point, the steady state can then be written as

$$\rho_{ss}^{(\vec{0},\vec{0})}(g = g_c) = c\rho_{1+}^{(\vec{0},\vec{0})} + (1 - c)\rho_{1-}^{(\vec{0},\vec{0})}, \quad (\text{S21})$$

¹ We recall that we always assume the diagonalizability of the HEOM Liouvillian.

where $c \in [0, 1]$. Now, for all $g \neq g_c$ and $g \in [g_c - \epsilon, g_c + \epsilon]$ ($\epsilon > 0$), the gap is not closed. Therefore,

$$\mathcal{P}^{(\vec{0}, \vec{0})} \lim_{g \rightarrow g_c^\pm} \lim_{t \rightarrow +\infty} e^{\mathcal{L}_{\text{HEOM}}(g)t} \rho_{1\pm}(g) = \lim_{g \rightarrow g_c^\pm} \rho_0^{(\vec{0}, \vec{0})}(g) = \lim_{g \rightarrow g_c^\pm} \rho_{ss}^{(\vec{0}, \vec{0})}(g), \quad (\text{S22})$$

By hypothesis, however, $\rho_{ss}^{(\vec{0}, \vec{0})}$ is continuous at $g = g_c$, which means

$$\mathcal{P}^{(\vec{0}, \vec{0})} \lim_{g \rightarrow g_c^\pm} \lim_{t \rightarrow +\infty} e^{\mathcal{L}_{\text{HEOM}}(g)t} \rho_{1\pm}(g) = \rho_{ss}^{(\vec{0}, \vec{0})}(g = g_c) = c\rho_{1+}^{(\vec{0}, \vec{0})} + (1 - c)\rho_{1-}^{(\vec{0}, \vec{0})}, \quad (\text{S23})$$

or

$$\rho_{1\pm}^{(\vec{0}, \vec{0})}(g = g_c) = c\rho_{1+}^{(\vec{0}, \vec{0})}(g = g_c) + (1 - c)\rho_{1-}^{(\vec{0}, \vec{0})}(g = g_c), \quad (\text{S24})$$

since $\rho_{1\pm}(g)$ belongs to the null space at $g = g_c$. From Eq. (S24) we infer $\rho_{1+}^{(\vec{0}, \vec{0})}(g = g_c) = \rho_{1-}^{(\vec{0}, \vec{0})}(g = g_c)$, hence the contradiction with $\langle\langle \rho_{1+}^{(\vec{0}, \vec{0})} | \rho_{1-}^{(\vec{0}, \vec{0})} \rangle\rangle \equiv \text{Tr}[\rho_{1+}^{(\vec{0}, \vec{0})\dagger} \rho_{1-}^{(\vec{0}, \vec{0})}] = 0$ or even with the very existence of $\rho_1^{(\vec{0}, \vec{0})}$. \square

2. 2nd-order DPTs with SSB

Let us now discuss the consequences of the properties of the HEOM Liouvillian on 2nd-order DPTs associated with SSB. For clarity, we only consider DPTs associated with a \mathbb{Z}_2 -SSB, but the generalization to more general symmetries is straightforward.

Let $\mathcal{L}_{\text{HEOM}}(g)$ be the HEOM generator that captures a 2nd-order DPT associated with the spontaneous breaking of a \mathbb{Z}_2 symmetry for $g \geq g_c$, g_c being the critical point. By definition of a weak symmetry, there exists a superoperator \mathcal{U}_2 such that

$$[\mathcal{L}_{\text{HEOM}}, \mathcal{U}_2] = 0. \quad (\text{S25})$$

As discussed in the main text, the very existence of the operator \mathcal{U}_2 constrains the HEOM generator to adopt a block-diagonal structure when written in the eigenbasis of \mathcal{U}_2 , namely

$$\mathcal{L}_{\text{HEOM}} = \bigoplus_{u_k = \pm 1} \mathcal{L}_{u_k}, \quad (\text{S26})$$

where $\mathcal{L}_{u_k = \pm 1}$ are the blocs associated with the two eigenvalues of \mathcal{U}_2 , namely ± 1 . By hypothesis, a 2nd-order DPT with \mathbb{Z}_2 -SSB occurs for $g \geq g_c$ and $N \rightarrow +\infty$ *i.e.*, the two blocks \mathcal{L}_{+1} ($k = 0$) and \mathcal{L}_{-1} ($k = 1$) get coupled in the thermodynamic limit: $\lambda_0^{(k=0)}(g \geq g_c) = 0 = \lambda_0^{(k=1)}$. The associated eigenvectors, denoted by $\rho_0^{(k)}$, are then orthogonal since we have

$$\langle\langle \rho_0^{(0)} | \rho_0^{(1)} \rangle\rangle = \langle\langle \mathcal{U}_2 \rho_0^{(0)} | \rho_0^{(1)} \rangle\rangle = \langle\langle \rho_0^{(0)} | \mathcal{U}_2 \rho_0^{(1)} \rangle\rangle = -\langle\langle \rho_0^{(0)} | \rho_0^{(1)} \rangle\rangle \quad (\text{S27})$$

as \mathcal{U}_2 is Hermitian, and thus $\langle\langle \rho_0^{(0)} | \rho_0^{(1)} \rangle\rangle = 0$. Now, if we define

$$\rho_\pm \propto \rho_0^{(0)} \pm \rho_0^{(1)}, \quad (\text{S28})$$

it is clear that ρ_\pm belong to the kernel of $\mathcal{L}_{\text{HEOM}}(g \geq g_c)$ in the thermodynamic limit. Note, however, that ρ_\pm are not eigenvectors of \mathcal{U}_2 as $\mathcal{U}_2 \rho_\pm \propto \rho_\mp$. Moreover, the projections $\rho_\pm^{(\vec{0}, \vec{0})} = \mathcal{P}^{(\vec{0}, \vec{0})} \rho_\pm$ allow us to interpret $\rho_\pm^{(\vec{0}, \vec{0})}$ as steady-states of the system that explicitly break the symmetry. Equation (S28) can be inverted, so that

$$\begin{aligned} \rho_0^{(0)} &\propto \rho_+ + \rho_-, \\ \rho_0^{(1)} &\propto \rho_+ - \rho_-. \end{aligned} \quad (\text{S29})$$

In particular, if we apply $\mathcal{P}^{(\vec{0}, \vec{0})}$ to both sides of the previous relations, we obtain

$$\begin{aligned} \rho_0^{(0)(\vec{0}, \vec{0})} &\propto \rho_+^{(\vec{0}, \vec{0})} + \rho_-^{(\vec{0}, \vec{0})}, \\ \rho_0^{(1)(\vec{0}, \vec{0})} &\propto \rho_+^{(\vec{0}, \vec{0})} - \rho_-^{(\vec{0}, \vec{0})}, \end{aligned} \quad (\text{S30})$$

with $\mathcal{P}^{(\vec{0},\vec{0})}\rho_0^{(k)} = \rho_0^{(k)(\vec{0},\vec{0})}$ ($k = 0, 1$), which is exactly what predicts the Markovian theory [S3]. For finite N , the steady-state is unique, *i.e.* $\rho_{ss} \propto \rho_0^{(0)(\vec{0},\vec{0})}$ and therefore

$$\rho_{ss}(g \geq g_c, N) \approx \frac{\rho_+^{(\vec{0},\vec{0})}(g \geq g_c, N) + \rho_-^{(\vec{0},\vec{0})}(g \geq g_c, N)}{2}. \quad (\text{S31})$$

In Sec. V.B, we checked numerically the validity of this decomposition for the second model considered in the main text.

IV. FIRST MODEL - SHIFTING PHASE BOUNDARIES VIA NON-MARKOVIAN EFFECTS

In this section, we present details on the first model we consider in the main text, *i.e.*, the generalized dissipative Lipkin-Meshkov-Glick model, which generalizes the study made in Ref. [S6] to the non-Markovian regime. The master equation for the collective spin and pseudo-mode density matrix reads [Eq. (8) in the main text]

$$\begin{aligned} \dot{\rho}_{\text{tot}} &= -i[H, \rho_{\text{tot}}] + \kappa (2a\rho_{\text{tot}}a^\dagger - \{a^\dagger a, \rho_{\text{tot}}\}) \\ \text{with } H &= H_{\text{LMG}} + \omega a^\dagger a + \sqrt{\frac{\gamma\kappa}{2N}} (S_- a^\dagger + a S_+). \end{aligned} \quad (\text{S32})$$

In the following, we first show how adiabatic elimination of the cavity mode recovers the original model [Eq.(7) in the main text] in the “bad cavity” limit before performing a mean-field analysis of our generalized model.

A. Adiabatic elimination of the cavity mode in the bad cavity limit

Let us perform a standard derivation of a master equation for the collective spin only, first dividing $H = H_0 + H_1$ and then working in the interaction picture with respect to $H_0 = H_{\text{LMG}} + \omega a^\dagger a$. In this interaction picture, the interaction Hamiltonian H_1 takes the form:

$$H_1(t) = \sqrt{\frac{\gamma\kappa}{2N}} (a(t)S_+(t) + a^\dagger(t)S_-(t)), \quad (\text{S33})$$

where $S_\pm(t) = e^{iH_{\text{LMG}}t} S_\pm e^{-iH_{\text{LMG}}t}$. The master equation for the collective spin density operator $\rho = \text{Tr}_E(\rho_{\text{tot}})$ reads in the Markov approximation [S7]:

$$\dot{\rho} = - \int_0^t dt' \text{Tr}_E ([H_1(t), [H_1(t'), \rho_{\text{tot}}(t)]]). \quad (\text{S34})$$

Considering the Born approximation $\rho_{\text{tot}}(t) \approx \rho(t) \otimes \rho_E$ with ρ_E the vacuum state for the pseudo mode and expanding the double commutator yields

$$\dot{\rho} = - \int_0^t dt' \left(\alpha(t-t') S_+(t) S_-(t') \rho(t) - \alpha^*(t-t') S_-(t) \rho(t) S_+(t') - \alpha(t-t') S_-(t') \rho(t) S_+(t) + \alpha^*(t-t') \rho(t) S_+(t') S_-(t) \right), \quad (\text{S35})$$

which made appear the bath correlation function

$$\alpha(t-t') = \left(\frac{\gamma\kappa}{2N} \right) \text{Tr}_E (a(t) a^\dagger(t') \rho_E) = \frac{\gamma\kappa}{2N} e^{-i\omega(t-t') - \kappa|t-t'|}. \quad (\text{S36})$$

a. “Bad cavity” limit $\kappa \rightarrow \infty$. In the “bad cavity” limit $\kappa \rightarrow \infty$, which corresponds to the case of a flat spectral density of the bath, we have $\alpha(t-t') \rightarrow (\gamma/N)\delta(t-t')$, which makes it possible to perform the integration straightforwardly and obtain the following master equation in the Schrödinger picture

$$\dot{\rho} = -i[H_{\text{LMG}}, \rho] + \frac{\gamma}{2N} (2S_- \rho S_+ - \{S_+ S_-, \rho\}), \quad (\text{S37})$$

which is exactly Eq. (7) in the main text.

b. Finite κ and large detuning limit. If we now consider the case of finite κ , the integrand in Eq. (S35) is non-zero over a finite range of time t' , so that one has in principle to know the explicit time-dependence of the system operators $S_{\pm}(t') = e^{iH_{\text{LMG}}t'} S_{\pm} e^{-iH_{\text{LMG}}t'}$ - and thus the H_{LMG} Hamiltonian spectrum - to perform the integral. Such knowledge is however not needed in the limit where the pseudo-mode frequency ω dominates all system transition frequencies as shown below. Suppose indeed a spectral decomposition of H_{LMG} of the form $H_{\text{LMG}}|n\rangle = \omega_n|n\rangle$ with eigenvalues and eigenvectors ω_n and $|n\rangle$. The time-dependence of the system operators $S_{\pm}(t')$ in the H_{LMG} Hamiltonian basis reads

$$S_{\pm}(t) = \sum_{n,n'} e^{-i(\omega_n - \omega_{n'})t} \langle n|S_{\pm}|n'\rangle |n\rangle\langle n'|. \quad (\text{S38})$$

Inserting Eq. (S38) in Eq. (S35), making the variable substitution $t' \rightarrow t - \tau$ and pushing the limit of the integral to infinity yields after integration

$$\begin{aligned} \dot{\rho} = & -\frac{\gamma\kappa}{2N} \sum_{n,n'} \left(\frac{1}{\kappa + i(\omega - (\omega_n - \omega_{n'}))} S_+(t) \left(e^{-i(\omega_n - \omega_{n'})t} \langle n|S_-|n'\rangle |n\rangle\langle n'| \right) \rho(t) \right. \\ & - \frac{1}{\kappa - i(\omega + (\omega_n - \omega_{n'}))} S_-(t) \rho(t) \left(e^{-i(\omega_n - \omega_{n'})t} \langle n|S_+|n'\rangle |n\rangle\langle n'| \right) \\ & - \frac{1}{\kappa + i(\omega - (\omega_n - \omega_{n'}))} \left(e^{-i(\omega_n - \omega_{n'})t} \langle n|S_-|n'\rangle |n\rangle\langle n'| \right) \rho(t) S_+(t) \\ & \left. + \frac{1}{\kappa - i(\omega + (\omega_n - \omega_{n'}))} \rho(t) \left(e^{-i(\omega_n - \omega_{n'})t} \langle n|S_+|n'\rangle |n\rangle\langle n'| \right) S_-(t) \right). \end{aligned} \quad (\text{S39})$$

If now we have $\omega \gg (\omega_n - \omega_{n'}) \forall n, n'$, then $1/(\kappa \pm i(\omega \pm (\omega_n - \omega_{n'}))) \approx 1/(\kappa \pm i\omega)$ and the equation becomes

$$\dot{\rho} = -\frac{\gamma\kappa}{2N} \left(\frac{1}{\kappa + i\omega} S_+(t) S_-(t) \rho(t) - \frac{1}{\kappa - i\omega} S_-(t) \rho(t) S_+(t) - \frac{1}{\kappa + i\omega} S_-(t) \rho(t) S_+(t) + \frac{1}{\kappa - i\omega} \rho(t) S_+(t) S_-(t) \right). \quad (\text{S40})$$

Coming back to the Schrödinger picture yields

$$\dot{\rho} = -i \left[H_{\text{LMG}} - q_2 \frac{\gamma}{2N} S_+ S_-, \rho \right] + q_1 \frac{\gamma}{2N} (2S_- \rho S_+ - \{S_+ S_-, \rho\}), \quad (\text{S41})$$

where we introduced the factors

$$q_1 = \frac{\kappa^2}{\kappa^2 + \omega^2}, \quad q_2 = \frac{\kappa\omega}{\kappa^2 + \omega^2}. \quad (\text{S42})$$

Hence, we see that in the large detuning limit $\omega/(\omega_n - \omega_{n'}) \rightarrow \infty \forall n, n'$, the structure of the bath spectral density has the effect of reducing the impact of the dissipative part of the master equation for the spin by a factor $q_1 = \kappa^2/(\kappa^2 + \omega^2)$ as well as adding a energy shift proportional to $q_2\gamma/2N$.

c. Redfield master equation. As explained above, going beyond the approximations used in the previous section require to take into account the spectrum of the system to evaluate the dissipative part of the master equation. However, the Lipkin-Meshkov-Glick Hamiltonian has complicated eigenvalues and eigenvectors [S8, S9] and it is not easy to write down simple formula for Eq. (S38), which hampers the writing of a simple expression for the master equation and strongly motivates the use of our systematic HEOM approach.

B. Mean-field analysis

We first start by writing the Heisenberg equations of motion for a , S_x , S_y and S_z from Eq. (S32)

$$\begin{aligned} \dot{a} &= -(\kappa + i\omega)a - i\sqrt{\frac{\gamma\kappa}{2N}} S_-, \\ \dot{S}_x &= -\frac{V}{N} \{S_y, S_z\} + i\sqrt{\frac{\gamma\kappa}{2N}} S_z (a - a^\dagger), \\ \dot{S}_y &= -\frac{V}{N} \{S_x, S_z\} - \sqrt{\frac{\gamma\kappa}{2N}} S_z (a + a^\dagger), \\ \dot{S}_z &= 2\frac{V}{N} \{S_x, S_y\} + i\sqrt{\frac{\gamma\kappa}{2N}} (a^\dagger S_- - a S_+). \end{aligned} \quad (\text{S43})$$

Using $\langle AB \rangle = \frac{1}{2} \langle \{A, B\} + [A, B] \rangle \approx \langle A \rangle \langle B \rangle + \frac{1}{2} \langle [A, B] \rangle$, we get the mean-field semiclassical equations of motion

$$\langle \dot{a} \rangle = -(\kappa + i\omega) \langle a \rangle - i \sqrt{\frac{\gamma\kappa}{2N}} \langle S_- \rangle, \quad (\text{S44})$$

$$\langle \dot{S}_x \rangle = -2 \frac{V}{N} \langle S_y \rangle \langle S_z \rangle + i \sqrt{\frac{\gamma\kappa}{2N}} \langle S_z \rangle (\langle a \rangle - \langle a^\dagger \rangle), \quad (\text{S45})$$

$$\langle \dot{S}_y \rangle = -2 \frac{V}{N} \langle S_x \rangle \langle S_z \rangle - \sqrt{\frac{\gamma\kappa}{2N}} \langle S_z \rangle (\langle a \rangle + \langle a^\dagger \rangle), \quad (\text{S46})$$

$$\langle \dot{S}_z \rangle = 4 \frac{V}{N} \langle S_x \rangle \langle S_y \rangle + i \sqrt{\frac{\gamma\kappa}{2N}} (\langle a^\dagger \rangle \langle S_- \rangle - \langle a \rangle \langle S_+ \rangle), \quad (\text{S47})$$

which are exact in the thermodynamic limit $N \rightarrow \infty$. Note that the quantity $\langle S_x \rangle^2 + \langle S_y \rangle^2 + \langle S_z \rangle^2$ is a constant of motion, hence the dynamics of the spin is constrained to the surface of a Bloch sphere. In the following, we are interested in finding the fixed points of these equations and studying their stability as a function of the parameters of the model, in order to deduce the different possible steady states and build a phase diagram as in [S6].

The different fixed points labelled as $\{(\langle a \rangle, \langle S_x \rangle, \langle S_y \rangle, \langle S_z \rangle)_*\}$ of Eqs. (S44)-(S47) can be obtained by setting the left-hand-side of all the equations to zero. In particular, from the first equation, setting $\langle \dot{a} \rangle = 0$ gives

$$\langle a \rangle_* = -i \frac{\sqrt{\frac{\gamma\kappa}{2N}} \langle S_- \rangle_*}{\kappa + i\omega} \quad (\text{S48})$$

Hence, the pseudo-mode degree of freedom is slaved to the collective spin ones, which simplifies the problem as we just need to find first the fixed points of a closed set of equations for the collective spin variables $\langle S_x \rangle_*$, $\langle S_y \rangle_*$ and $\langle S_z \rangle_*$ only, i.e.,

$$0 = -2 \frac{V}{N} \langle S_y \rangle_* \langle S_z \rangle_* + \frac{\gamma}{N} \langle S_z \rangle_* (q_1 \langle S_x \rangle_* - q_2 \langle S_y \rangle_*), \quad (\text{S49})$$

$$0 = -2 \frac{V}{N} \langle S_x \rangle_* \langle S_z \rangle_* + \frac{\gamma}{N} \langle S_z \rangle_* (q_1 \langle S_y \rangle_* + q_2 \langle S_x \rangle_*), \quad (\text{S50})$$

$$0 = 4 \frac{V}{N} \langle S_x \rangle_* \langle S_y \rangle_* - \frac{\gamma}{N} q_1 (\langle S_x \rangle_*^2 + \langle S_y \rangle_*^2). \quad (\text{S51})$$

It is worth noting that if one is interested in deriving a spin-only description of the model by performing an adiabatic elimination of the pseudo mode (as done in the case of the Dicke model in [S10]), it would also require to setting $\dot{a} = 0$ in Eqs. (S44)-(S47), which would yield Eqs. (S49)-(S51) but with the derivative of the collective spin operators on the left-hand-sides of each equation. Importantly, this means the fixed points of the spin system after adiabatic elimination of the pseudo mode are the same as the full model. However, as we will see below, their stability differs depending on whether or not we account for the pseudo-mode degree of freedom. Note also that taking the limit $\kappa/\omega \rightarrow \infty$ in Eqs. (S49)-(S51) yields $q_1 \rightarrow 1$ and $q_2 \rightarrow 0$, so that we recover the semiclassical equations of the Lindblad model [S6].

Equations (S49)-(S51) together with the normalization condition $\langle S_x \rangle_*^2 + \langle S_y \rangle_*^2 + \langle S_z \rangle_*^2 = (N/2)^2$ admit (as for the Markovian case) two classes of fixed points:

$$(\langle S_x \rangle, \langle S_y \rangle, \langle S_z \rangle)_* = \frac{N}{2} (0, 0, \pm 1) \quad (\text{S52})$$

and

$$(\langle S_x \rangle, \langle S_y \rangle, \langle S_z \rangle)_* = \frac{N}{2} \left(\frac{\sqrt{1 \pm \sqrt{1 - \frac{q_1^2 \gamma^2}{4V^2}}}}{\sqrt{2}}, \frac{q_1 \gamma}{4V} \frac{\sqrt{2}}{\sqrt{1 \pm \sqrt{1 - \frac{q_1^2 \gamma^2}{4V^2}}}}, 0 \right), \quad (\text{S53})$$

$$(\langle S_x \rangle, \langle S_y \rangle, \langle S_z \rangle)_* = -\frac{N}{2} \left(\frac{\sqrt{1 \pm \sqrt{1 - \frac{q_1^2 \gamma^2}{4V^2}}}}{\sqrt{2}}, \frac{q_1 \gamma}{4V} \frac{\sqrt{2}}{\sqrt{1 \pm \sqrt{1 - \frac{q_1^2 \gamma^2}{4V^2}}}}, 0 \right). \quad (\text{S54})$$

According to Eq. (S48), the first class of fixed points corresponds to the spin at the north and south poles of the Bloch sphere with an empty pseudo mode, while the second class of fixed points corresponds to the spin at four different locations at the equator and a scaling $\langle a \rangle_* \propto \sqrt{N}$ for the pseudo mode. In the following, we analyse the stability of these fixed points to determine the steady states of the model. As it turns out that it depends on whether the analysis is performed on the spin degrees of freedom (S_x, S_y, S_z) only (spin model), as obtained from adiabatic elimination of the pseudo mode, or on all degrees of freedom (a, S_x, S_y, S_z) (full model), we investigate subsequently these two cases.

1. Spin model

a. Linear stability analysis. Let us first perform a linear stability analysis for the spin model obtained after adiabatic elimination of the pseudo mode, i.e.,

$$\langle \dot{S}_x \rangle = -2\frac{V}{N}\langle S_y \rangle \langle S_z \rangle + \frac{\gamma}{N}\langle S_z \rangle (q_1 \langle S_x \rangle - q_2 \langle S_y \rangle), \quad (\text{S55})$$

$$\langle \dot{S}_y \rangle = -2\frac{V}{N}\langle S_x \rangle \langle S_z \rangle + \frac{\gamma}{N}\langle S_z \rangle (q_1 \langle S_y \rangle + q_2 \langle S_x \rangle), \quad (\text{S56})$$

$$\langle \dot{S}_z \rangle = 4\frac{V}{N}\langle S_x \rangle \langle S_y \rangle - \frac{\gamma}{N}q_1 (\langle S_x \rangle^2 + \langle S_y \rangle^2), \quad (\text{S57})$$

around the first class of fixed points: $(\langle S_x \rangle, \langle S_y \rangle, \langle S_z \rangle)_* = (0, 0, \pm N/2)$. Note that the equations above can also be obtained from the master equation (S41) in the large detuning limit. To perform the analysis, we replace $(\langle S_x \rangle, \langle S_y \rangle, \langle S_z \rangle)$ by $(x, y, z \pm (N/2))$ in Eqs. (S55-S57) where (x, y, z) denotes fluctuations around the fixed points which yields

$$\dot{x} = -2\frac{V}{N}y \left(z \pm \frac{N}{2} \right) + \frac{\gamma}{N} \left(z \pm \frac{N}{2} \right) (q_1 x - q_2 y), \quad (\text{S58})$$

$$\dot{y} = -2\frac{V}{N}x \left(z \pm \frac{N}{2} \right) + \frac{\gamma}{N} \left(z \pm \frac{N}{2} \right) (q_1 y + q_2 x), \quad (\text{S59})$$

$$\dot{z} = 4\frac{V}{N}xy - \frac{\gamma}{N}q_1 (x^2 + y^2). \quad (\text{S60})$$

Linearizing Eqs. (S58)-(S60) shows that fluctuations along z decouple from those along x and y , which reduces the analysis to the following two-dimensional system

$$\begin{pmatrix} \dot{x} \\ \dot{y} \end{pmatrix} = \pm \frac{\gamma}{2} \begin{pmatrix} q_1 & -\frac{2V}{\gamma} - q_2 \\ -\frac{2V}{\gamma} + q_2 & q_1 \end{pmatrix} \begin{pmatrix} x \\ y \end{pmatrix}. \quad (\text{S61})$$

The eigenvalues of the matrix are $\pm\gamma(q_1 - \sqrt{4(V/\gamma)^2 - q_2^2})/2$ and $\pm\gamma(q_1 + \sqrt{4(V/\gamma)^2 - q_2^2})/2$. For the fixed point $(\langle S_x \rangle, \langle S_y \rangle, \langle S_z \rangle)_* = (0, 0, \frac{N}{2})$ [“+” sign in Eq. (S61)], the eigenvalue $\gamma(q_1 + \sqrt{4(V/\gamma)^2 - q_2^2})/2$ is always positive, meaning that the fixed point is always unstable. For the fixed point $(\langle S_x \rangle, \langle S_y \rangle, \langle S_z \rangle)_* = (0, 0, -\frac{N}{2})$ [“-” sign in Eq. (S61)], both the eigenvalues $-\gamma(q_1 - \sqrt{4(V/\gamma)^2 - q_2^2})/2$ and $-\gamma(q_1 + \sqrt{4(V/\gamma)^2 - q_2^2})/2$ are negative for

$$V < \frac{\gamma}{2\sqrt{1 + \omega^2/\kappa^2}} \equiv V_c^+, \quad (\text{S62})$$

and $-\gamma(q_1 - \sqrt{4(V/\gamma)^2 - q_2^2})/2$ is positive for $V > V_c^+$. Hence, the fixed point $(\langle S_x \rangle, \langle S_y \rangle, \langle S_z \rangle)_* = (0, 0, -\frac{N}{2})$ is stable only if $V < V_c^+$ and unstable otherwise. Note again that in the limit $\kappa/\omega \rightarrow \infty$, we recover the result of the Lindblad model of [S6] where $V_c^+ \rightarrow \gamma/2$.

Let us now perform a linear stability analysis around the second class of fixed points of the form $(\langle S_x \rangle, \langle S_y \rangle, \langle S_z \rangle)_* = (s_{x*}, s_{y*}, 0)$, where s_{x*} and s_{y*} are given by the right-hand side of Eqs. (S53) or (S54). Here, the EOM for the fluctuations, obtained by replacing $(\langle S_x \rangle, \langle S_y \rangle, \langle S_z \rangle)$ by $(x + s_{x*}, y + s_{y*}, z)$, yields after linearization

$$\begin{pmatrix} \dot{x} \\ \dot{y} \\ \dot{z} \end{pmatrix} = \frac{1}{N} \begin{pmatrix} 0 & 0 & q_1 \gamma s_{x*} - (2V + q_2 \gamma) s_{y*} \\ 0 & 0 & q_1 \gamma s_{y*} - (2V - q_2 \gamma) s_{x*} \\ 4V s_{y*} - 2q_1 \gamma s_{x*} & 4V s_{x*} - 2q_1 \gamma s_{y*} & 0 \end{pmatrix} \begin{pmatrix} x \\ y \\ z \end{pmatrix} + \begin{pmatrix} 0 \\ 0 \\ -\frac{N\gamma q_1}{4} \end{pmatrix}. \quad (\text{S63})$$

The eigenvalues of the matrix are

$$0, \quad -N\sqrt{(\pm q_2 \sqrt{4V^2 - \gamma^2 q_1^2} + \gamma^2 q_1^2 - 4V^2)/2}, \quad \text{and} \quad N\sqrt{(\pm q_2 \sqrt{4V^2 - \gamma^2 q_1^2} + \gamma^2 q_1^2 - 4V^2)/2}, \quad (\text{S64})$$

where the \pm sign relate to the \pm sign in Eqs. (S53) and (S54). Note that the zero eigenvalue is not physical, as the variables are not independent. To see how this eigenvalue can be eliminated, one can switch to the spherical coordinates $\langle S_x \rangle = r \sin \theta \cos \varphi$, $\langle S_y \rangle = r \sin \theta \sin \varphi$, $\langle S_z \rangle = r \cos \theta$ in Eqs. (S55-S57), which yields $\dot{r} = 0$ because of the norm conservation and

$$\dot{\varphi} = \frac{\cos \theta}{2} [q_2 \gamma - 2V \cos(2\varphi)], \quad (\text{S65})$$

$$\dot{\theta} = \frac{\sin \theta}{2} [q_1 \gamma - 2V \sin(2\varphi)]. \quad (\text{S66})$$

Linear stability analysis based on these equations yields the two non-trivial eigenvalues of Eq. (S64). The fixed points are unstable when the real part of at least one of them is positive. This happens for

$$V < \frac{\gamma}{2(1 + \omega^2/\kappa^2)} \equiv V_c^- \quad (\text{S67})$$

for the two fixed points associated with the “-” sign in Eqs. (S53) and (S54) and for

$$V < V_c^+ \quad (\text{S68})$$

for the two fixed points associated with the “+” sign. Above these critical values, the real part of both the eigenvalues are zero, and so one cannot conclude on the stability of the fixed points in this region via this simple linear stability analysis.

While the approach above cannot provide a full understanding of the stability of the system, we already see strong deviations from the Markovian limit $\omega/\kappa \rightarrow 0$. Indeed, in this latter, we have $V_c^- = V_c^+ = V_c^M = \gamma/2$ so that there is no region of parameters where the two kind of fixed points are not unstable, hampering the possibility for a coexistence of two distinct phases. More specifically, in [S6], it was shown that for $V < V_c^M$ the fixed point $(0, 0, -N/2)$ is the unique steady state while for $V > V_c^M$ the fixed points $(s_{x*}, s_{y*}, 0)$ are center fixed points and there exists an infinite set of oscillating (initial-state-dependent) steady states corresponding to orbits around these fixed points on the Bloch sphere. While these steady states are persistent spin oscillations, they average to zero along the z direction over time, so that the Markovian scenario well-describes a 1st-order transition between a phase with $\langle S_z \rangle \neq 0$ ($V < V_c^M$) and $\langle S_z \rangle = 0$ ($V > V_c^M$). In the case $\omega/\kappa \neq 0$, however, we have $V_c^- < V_c^+$, so the possibility that the fixed points and thus two distinct phases coexist in the region $V_c^- < V < V_c^+$ (which increases as ω/κ increases) is not excluded. This is confirmed in the next subsection.

b. Higher-order stability analysis. As the equations of motion are cumbersome beyond linearization, we rely on a numerical analysis of the stability of the fixed points, as summarized below.

For $0 \leq V < V_c^-$, the fixed point $(0, 0, -N/2)$ is the unique steady state, as shown in the stream plots in Fig. S3 (a,b,e). Note that in this regime all the fixed points of the form $(s_{x*}, s_{y*}, 0)$ are not physical fixed points as they are complex vectors.

For $V_c^- < V < V_c^+$, we observe a bistability phenomenon as the steady state depends on the initial conditions: the fixed point $(0, 0, -N/2)$ is still a possible steady state, but an infinite number of steady states corresponding to stable orbits on the Bloch sphere around the two center fixed points (S53) and (S54) with the “-” sign become available, as shown in Fig. S3(f). For $V \gtrsim V_c^-$, only orbits close to the fixed points are stable. As V increases, more orbits become stable. This is in sharp contrast with the Markovian case where all the points on the sphere belong to stable orbits as soon as $V > V_c^M$ [panel (c,d)]. Here, in the regime $V_c^- < V < V_c^+$, each point on the Bloch sphere undergoes the phase transition at a different critical point.

For $V > V_c^+$, the fixed point $(0, 0, -N/2)$ is no longer stable and all the four fixed points (S53) and (S54) become center fixed points, as can be seen in Fig. S3(g,h). Note that since $V_c^- < V_c^+$, this means going beyond the limit of a flat spectral density has the effect to renormalize to lower values the critical point by a function of the bath SD. We interpret this phenomenon as a consequence of memory effects: for smaller κ/ω , the excitations escaping the system are more likely to be re-absorbed by the system at later times, protecting its coherence and hence stabilizing the phase dominated by the Hamiltonian term to lower ratio V/γ .

2. Full model

We now come back to the mean-field equations for the full model (S44)-(S47) in order to study how reintroducing the pseudo-mode degree of freedom affects the stability of the fixed points. Here, the complex variable $\langle a \rangle$ can be decomposed into two real variables. Hence, the linear stability analysis on the full model exhibits four non-trivial eigenvalues to analyze, by contrast with the two of the previous section. As before, the analysis consists in linearizing

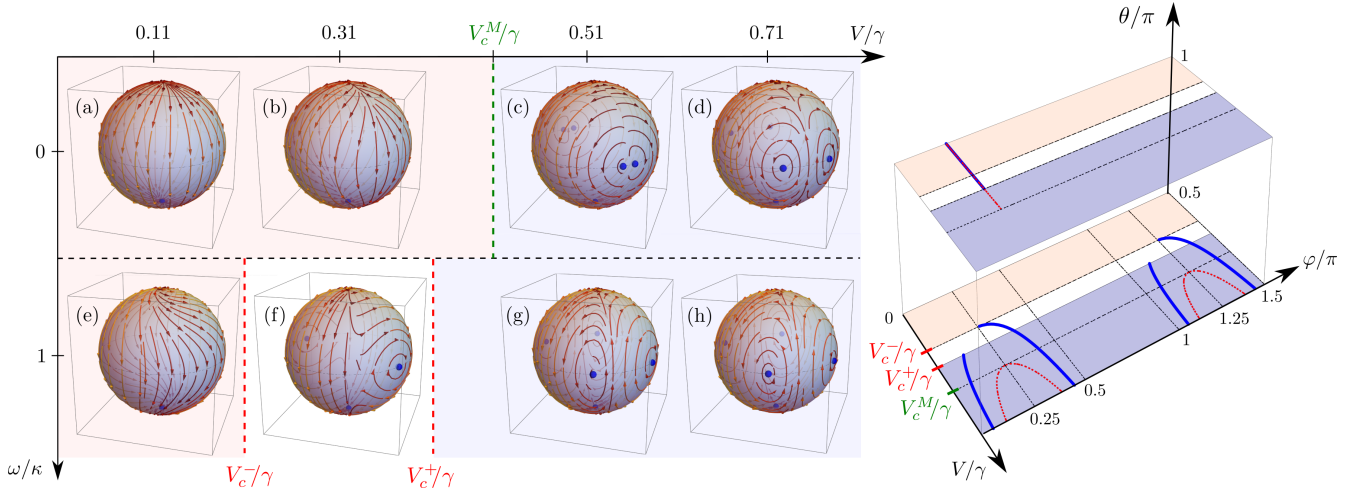


FIG. S3. Stream plots obtained from the mean-field equations (S55)-(S57) after adiabatic elimination of the pseudo mode showing the trajectories of the collective spin on the Bloch sphere in the thermodynamic limit as a function of the ratio V/γ between coherent and dissipative rates (not in scale) and of the degree of spectral density structures ω/κ . In the Markovian limit ($\omega/\kappa \rightarrow 0$), there is a phase transition at $V = V_c^M = \gamma/2$ between a phase with a unique pure steady state $(0, 0, -N/2)$ (blue dot at the south pole) [$V < V_c^M$, (a,b)] and a phase with an infinite set of (initial-state-dependent) pure steady states orbiting around four center fixed points (blue dots at the equator) [$V > V_c^M$, (c,d)]. As ω/κ increases, the stream lines twist around the z -axis (e) and a region of parameters ($V_c^- < V < V_c^+$) emerges where both the steady state $(0, 0, -N/2)$ or a steady orbit can be observed depending on the initial condition (f). Overall, the phase space where the coherent dynamics dominates over the dissipative one is enlarged due to non-Markovian effects. Parameters are $V/\gamma = 0.11$ (a,e), $V/\gamma = 0.31$ (b,f), $V/\gamma = 0.51$ (c,g) and $V/\gamma = 0.71$ (d,h). For $\omega/\kappa = 1$, $V_c^-/\gamma = 0.25$ and $V_c^+/\gamma \approx 0.354$. (i) Positions of the relevant fixed points on the Bloch sphere as a function of spherical coordinates φ and θ and V/γ for the Markovian limit $\omega/\kappa = 0$ (dashed red) and for $\omega/\kappa = 1$ (blue).

the equations of motion for the fluctuations around the different fixed points and inspecting the eigenvalues of the matrix of the system. We summarize below the results for each class of fixed points.

For the first class of fixed points at the north and south poles of the Bloch sphere, $(\langle S_x \rangle_*, \langle S_y \rangle_*, \langle S_z \rangle_*) = (0, 0, N/2)$ is still unstable for all values of V , while $(0, 0, -N/2)$ is still a valid steady state for $V < V_c^+$, as can be seen in panel (a) and (b) respectively of Fig. S4, which displays the real parts of the eigenvalues of the linear stability analysis matrix in each case.

For the second class of fixed points at the equator of the Bloch sphere, the changes are more drastic. (i) The two fixed points associated with the “-” sign in Eqs. (S53) and (S54) are still unstable for $V < V_c^-$. However, they are now *stable* for $V > V_c^-$, as can be seen in Fig. S4(c) showing that all real parts of the eigenvalues become negative in this region (blue solid curve), by contrast with the analysis of the reduced spin model (dashed purple and dotted dark cyan). Hence, these two fixed points are now real steady states for $V > V_c^-$, and they coexist with the steady state $(0, 0, -N/2)$ for $V_c^- < V < V_c^+$. There are no more stable orbits around these fixed points. (ii) The two fixed points associated with the “+” sign in Eqs. (S53) and (S54) are still unstable for $V < V_c^+$, and now become also unstable above V_c^+ , as can be seen in Fig. S4(d).

In conclusion, the mean-field analysis of our generalized LMG model (S32) yields qualitatively different phase diagrams depending on the approximations used.

- The original spin-only model of [S6] as obtained in the limit $\omega/\kappa \rightarrow 0$ exhibits the DPT at $V = V_c^M = \gamma/2$. For $V < \gamma/2$, $(0, 0, -N/2)$ is the only steady state, while for $V > \gamma/2$ they are four center fixed points at the equator of the Bloch sphere around which an infinity of stable orbits are valid steady states, which one is chosen depends on the initial conditions.
- When including the spectral structures of the bath in the reduced description of the spin system ($\omega/\kappa \neq 0$), the critical point is split into two: $V_c^- = \gamma/[2(1 + \omega^2/\kappa^2)]$ and $V_c^+ = \gamma/(2\sqrt{1 + \omega^2/\kappa^2})$ where $V_c^- < V_c^+$, and the four fixed points at the equator have shifted locations. For $V < V_c^-$, $(0, 0, -N/2)$ is the only steady state. For $V_c^- < V < V_c^+$, $(0, 0, -N/2)$ and an ensemble of stable orbits around two out of the four center fixed points can be steady states. For $V > V_c^+$, only stable orbits around the four center fixed points are steady states.
- In the exact full model, the fixed points remain the same but not their stability. Notably, stable orbit cannot be seen anymore in any regime. For $V < V_c^-$, $(0, 0, -N/2)$ is the only steady state. For $V_c^- < V < V_c^+$,

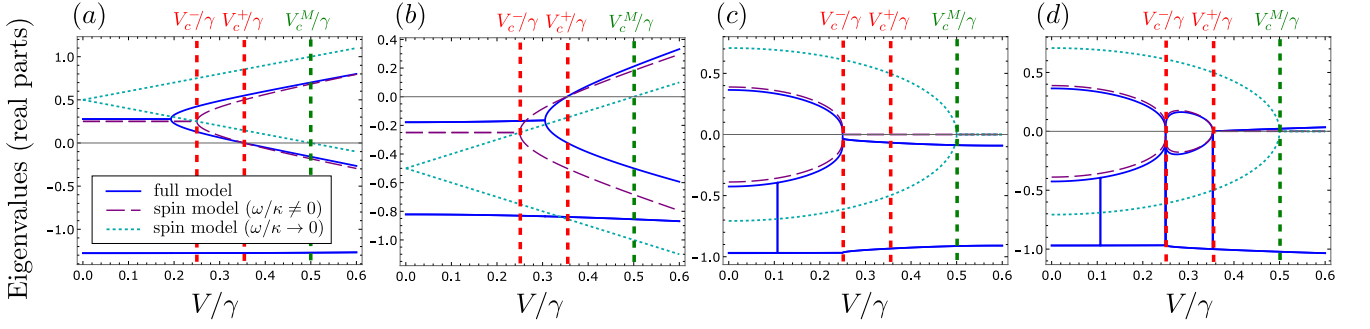


FIG. S4. Real parts of the eigenvalues of the linear stability analysis matrix of the mean-field equations for the full model [Eqs (S44)-(S47)] (blue solid lines) with $\omega = \kappa = \gamma$ and for the spin model after adiabatic elimination of the pseudo mode [Eqs. (S55)-(S57)] (dashed purple lines) with $\omega = \kappa = \gamma$ and in the limit $\omega/\kappa \rightarrow 0$ (dotted dark cyan lines). The different panels correspond to linear stability analyses around different fixed points: at the north pole of the Bloch sphere [$(\langle S_x \rangle, \langle S_y \rangle, \langle S_z \rangle)_* = (0, 0, -N/2)$] (a), at the south pole [$(0, 0, -N/2)$] (b) and at the equators [Eqs. (S53)-(S54) with the “-” sign (c) and the “+” sign (d)]. For a given V/γ , the fixed points are stable if all the corresponding eigenvalues have a negative real parts, while they are unstable if at least one of them is positive. The vertical dashed lines indicate the positions of the special values of V/γ as described in the text.

$(0, 0, -N/2)$ and two fixed points at the equator can be steady states. For $V > V_c^+$, only these two latter can be steady states.

Signatures of this overall picture can be found within our HEOM approach, as it predicts for finite N a transition between V_c^- and V_c^+ . We elaborate on this in the next section.

C. Understanding the emergence of 1st-order DPTs with spectral decompositions

Here, we illustrate on our first LMG model the extension of the Markovian theory of DPTs [S3] to the non-Markovian regime [see Sec. III. B.].

We have proven that the emergence of a DPT can be traced back to the existence of an eigenvalue $\lambda_1^{(0)}$ which vanishes at the critical point and in the thermodynamic limit $N \rightarrow +\infty$. Moreover, the associated eigenvector, namely ρ_1 whose projection on the system sector $(\vec{0}, \vec{0})$ is written $\rho_1^{(\vec{0}, \vec{0})}$, contains information about the system states right after/before the critical point, respectively denoted by $\rho_+^{(\vec{0}, \vec{0})}$ and $\rho_-^{(\vec{0}, \vec{0})}$. We also know that the steady state at the critical point can simply be written as a mixture with equal weights of the two phases $\rho_{\pm}^{(\vec{0}, \vec{0})}$. Those statements strictly hold true in the thermodynamic limit $N \rightarrow +\infty$. We expect, however, that at finite N the approximation

$$\rho_{ss}^{(\vec{0}, \vec{0})}(V = V_c, N) \approx \frac{\rho_+^{(\vec{0}, \vec{0})}(V_c, N) + \rho_-^{(\vec{0}, \vec{0})}(V_c, N)}{2}, \quad (\text{S69})$$

holds in a finite region around V_c and improves in accuracy as N increases. As in Sec. III. B, $\rho_{\pm}^{(\vec{0}, \vec{0})}(V_c, N)$ can be determined through the spectral decomposition $\rho_1^{(\vec{0}, \vec{0})}(V_c, N) \propto \rho_+^{(\vec{0}, \vec{0})}(V_c, N) - \rho_-^{(\vec{0}, \vec{0})}(V_c, N)$. Furthermore, as we approach the thermodynamic limit, the states $\rho_{\pm}^{(\vec{0}, \vec{0})}(V_c, N)$ are expected to approach the states immediately before or after the critical point.

In Fig. S5, we show the true quantum solution obtained through diagonalization of the HEOM generator and compare it with the states $\rho_{\pm}^{(\vec{0}, \vec{0})}$ and $(\rho_+^{(\vec{0}, \vec{0})} + \rho_-^{(\vec{0}, \vec{0})})/2$ as a function of V/γ and for two different values of N . As expected, the states $\rho_-^{(\vec{0}, \vec{0})}$ and $\rho_+^{(\vec{0}, \vec{0})}$ capture the right magnetization before and after the critical point, as shown in panels (b) and (c). We also investigate the fidelity between $\rho_{ss}^{(\vec{0}, \vec{0})}$ and the states $\rho_{\pm}^{(\vec{0}, \vec{0})}$, $(\rho_+^{(\vec{0}, \vec{0})} + \rho_-^{(\vec{0}, \vec{0})})/2$. We use the definition

$$F(A, B) = \text{Tr} \sqrt{\sqrt{AB}\sqrt{A}} \quad (\text{S70})$$

for the fidelity between density operators A and B . We find that $\rho_-^{(\vec{0}, \vec{0})}$ ($\rho_+^{(\vec{0}, \vec{0})}$) is a good approximation of the true steady state $\rho_{ss}^{(\vec{0}, \vec{0})}$ in a region below (above) the critical point. Moreover, in a small region around the critical point,

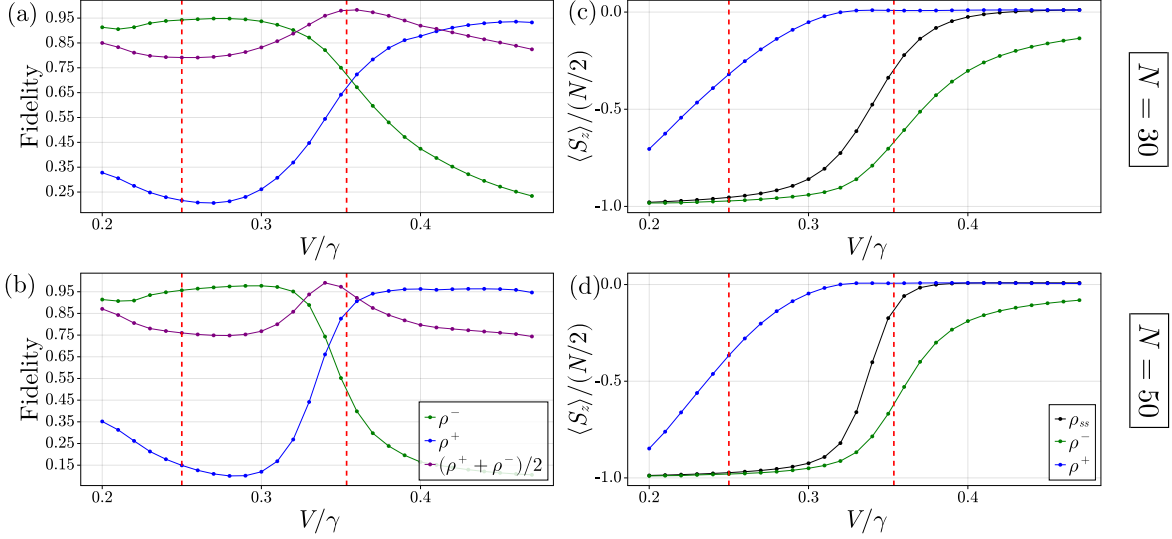


FIG. S5. Left panels: Fidelity between the steady states $\rho_{ss}^{\vec{0},\vec{0}}$ and the states $\rho_{\pm}^{\vec{0},\vec{0}}$ (green and blue curves) and $(\rho_+^{\vec{0},\vec{0}} + \rho_-^{\vec{0},\vec{0}})/2$ (purple curve) reconstructed from the spectral decomposition of $\rho_1^{\vec{0},\vec{0}}$. Right panels: Magnetization $\langle S_z \rangle / (N/2)$ as a function of V/γ for the steady state $\rho_{ss}^{\vec{0},\vec{0}}$ (black), $\rho_-^{\vec{0},\vec{0}}$ (green), $\rho_+^{\vec{0},\vec{0}}$ (blue). Panels (a) and (b) corresponds to $N = 30$ while panels (c) and (d) corresponds to $N = 50$. The parameters are the same of those of Fig. 2 of the main text.

the steady states is best described by $(\rho_+^{\vec{0},\vec{0}} + \rho_-^{\vec{0},\vec{0}})/2$. All these results are what we expect for finite N ; as N increases, we see that the region in which $(\rho_+^{\vec{0},\vec{0}} + \rho_-^{\vec{0},\vec{0}})/2 \approx \rho_{ss}^{\vec{0},\vec{0}}$ is getting narrower [compare panels (a) and (c)], which is consistent with the fact that Eq. (S69) strictly holds at a unique point in the thermodynamic limit. Finally, we note that the localization of the critical point get shifted as N increases while the fidelities get higher.

D. Impact of non-Markovianity on the critical point

In the main text, we showed that for the first LMG model we consider one can reshape the phase boundaries by considering a bath correlation function that decays with a finite time $1/\kappa$. In this section, we study more thoroughly the impact of this finite decay time on the DPT.

We find that the smaller κ/ω , the sharper the transition for a given N as illustrated by the panels (a)-(f) of Fig. S6. This result is not surprising as lowering κ/ω takes us further from the Markovian limit defined by $\kappa \rightarrow +\infty$, which in turn leads to larger values of k_{\max} to ensure convergence. However, as k_{\max} grows, the dimension of the HEOM Liouvillian $\mathcal{L}_{\text{HEOM}}$ also increases, in close analogy with the thermodynamic limit $N \rightarrow +\infty$ which also increases the dimension of the HEOM Liouvillian. The panel (g) of Fig. S6 shows that the critical point, numerically extracted from $\mathcal{L}_{\text{HEOM}}$ is always between V_c^+ and V_c^- for all values of κ/ω considered here, as expected. Furthermore, the critical point V_c/γ seems to more closely follow the scaling of V_c^+/γ given in Eq. (S62) than that of V_c^-/γ .

V. SECOND MODEL - TRIGGERING DPTS VIA NON-MARKOVIAN EFFECTS

This section is concerned with the second model considered in the main text, *i.e.* the modified LMG model coupled to a bath with exponentially decaying correlation function, which can be modelled as a spin system coupled to a damped pseudo-mode a .

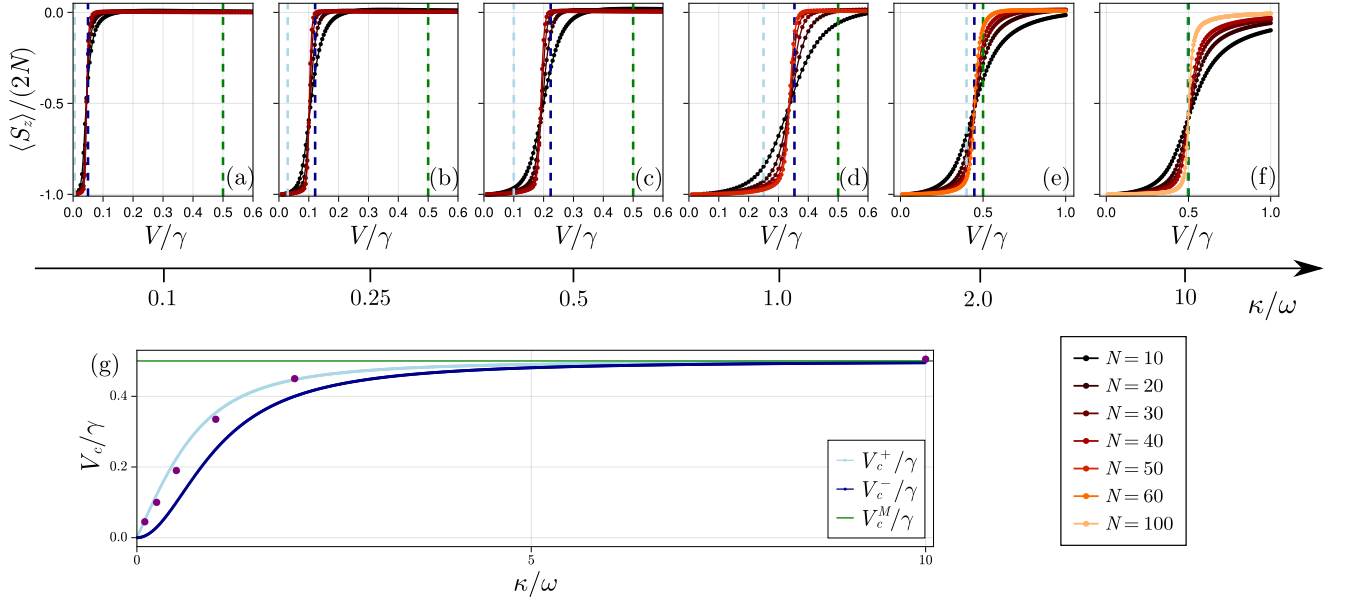


FIG. S6. Panels (a)-(f): Magnetization $\langle S_z \rangle / (2N)$ as a function of V/γ for different values of κ/ω [see axis below the plots] and for different values of N [see legend] highlighting the reshaping of the phase boundaries induced by non-Markovianity. Panel (g): Effective critical point V_c/γ (dots in purple), *i.e.* the critical point numerically found from $\mathcal{L}_{\text{HEOM}}$, as a function of κ/ω . We see that V_c/γ is always between $V_c^+\gamma$ and V_c^-/γ and appears to closely follow the scaling of V_c^+/γ given in Eq. (S62).

A. Mean-field analysis

In this section, we analyze the mean-field equations associated with the second model considered in the main text. The master equation for total density matrix reads

$$\begin{aligned} \dot{\rho}_{\text{tot}} &= -i[H, \rho_{\text{tot}}] + \kappa (2a\rho_{\text{tot}}a^\dagger - \{a^\dagger a, \rho_{\text{tot}}\}) \\ \text{with } H &= H_{\text{LMG}} + hS_z + \sqrt{\frac{\gamma\kappa}{2N}} S_x (a + a^\dagger). \end{aligned} \quad (\text{S71})$$

In close analogy with Section IV. B., it is easy to show that the mean-field equations read

$$\langle \dot{a} \rangle = -(\kappa + i\omega)\langle a \rangle - i\sqrt{\frac{\gamma\kappa}{2N}}\langle S_x \rangle, \quad (\text{S72})$$

$$\langle \dot{S}_x \rangle = -2\frac{V}{N}\langle S_y \rangle \langle S_z \rangle - h\langle S_y \rangle, \quad (\text{S73})$$

$$\langle \dot{S}_y \rangle = -2\frac{V}{N}\langle S_x \rangle \langle S_z \rangle + h\langle S_x \rangle - \sqrt{\frac{\gamma\kappa}{2N}}\langle S_z \rangle (\langle a \rangle + \langle a^\dagger \rangle), \quad (\text{S74})$$

$$\langle \dot{S}_z \rangle = 4\frac{V}{N}\langle S_x \rangle \langle S_y \rangle + \sqrt{\frac{\gamma\kappa}{2N}}\langle S_y \rangle (\langle a \rangle + \langle a^\dagger \rangle). \quad (\text{S75})$$

They have six fixed points from which four phases labelled as (I), (II), (IIb) and (III) can be inferred:

$$(I): (\langle a \rangle, \langle S_x \rangle, \langle S_y \rangle, \langle S_z \rangle)_* = \frac{N}{2} \left(\mp \sqrt{\frac{\gamma}{2N\kappa}} \sqrt{1 - \left(\frac{h}{V - \frac{q_2\gamma}{2}} \right)^2} (q_2 + iq_1), \pm \sqrt{1 - \left(\frac{h}{V - \frac{q_2\gamma}{2}} \right)^2}, 0, \frac{h}{\left(V - \frac{q_2\gamma}{2} \right)} \right) \quad (S76)$$

$$(II): (\langle a \rangle, \langle S_x \rangle, \langle S_y \rangle, \langle S_z \rangle)_* = \frac{N}{2} (0, 0, 0, -1) \quad (S77)$$

$$(IIb): (\langle a \rangle, \langle S_x \rangle, \langle S_y \rangle, \langle S_z \rangle)_* = \frac{N}{2} (0, 0, 0, 1) \quad (S78)$$

$$(III): (\langle a \rangle, \langle S_x \rangle, \langle S_y \rangle, \langle S_z \rangle)_* = \frac{N}{2} \left(0, 0, \pm \sqrt{1 - \left(\frac{h}{V} \right)^2}, -\frac{h}{V} \right). \quad (S79)$$

If $h > 0$ ($h < 0$), the phase (IIb) [(II)] is always unstable. As we chose $h > 0$ in the main text, we thus only have the phases (I), (II), and (III) to consider. Phases (I) and (III) both gather two fixed points, corresponding in each case to two broken symmetry states. Also, we note that their fixed points are unphysical for $|V - q_2\gamma/2| < h$ and $|V| < h$, respectively, which already gives some hints about their stability. A linear stability analysis around the fixed points show that the phases are stable in distinct regions of parameters. For $h, q_2, \gamma > 0$ as considered in the main text, we have the two critical points $V_1 = \min(-h + \frac{q_2\gamma}{2}, \frac{q_2\gamma}{4})$ and $V_2 = \max(h, \frac{q_2\gamma}{4})$ with phase (I) stable for $V < V_1$; phase (II) stable for $V_1 < V < V_2$; and phase (III) stable for $V_2 < V$. For $h > q_2\gamma/4$, the two critical points coalesce and phase (II) does not emerge anymore when varying V . In the particular case $\omega = \kappa = 2\gamma = 2h$ as considered in the main text, we have $V_1 = -3\gamma/4$ and $V_2 = \gamma$.

B. Understanding the emergence of 2nd-order DPT from spectral decompositions

In this section, we illustrate the validity of the spectral decomposition (S31), namely

$$\rho_{ss}(V, N) \approx \frac{\rho_+^{(\vec{0}, \vec{0})}(V, N) + \rho_-^{(\vec{0}, \vec{0})}(V, N)}{2}, \quad (S80)$$

for the model discussed above. Equation. (S80) should hold in phases where the \mathbb{Z}_2 symmetry is broken, *i.e.*, in phases (I) and (III), for large but finite N . Note, however, that the explicit construction of $\rho_{\pm}^{(\vec{0}, \vec{0})}$ requires $\lambda_0^{(1)}$ to be real such that the associated eigenvector is Hermitian. The imaginary part of this eigenvalue should vanish after the critical point in the thermodynamic limit because of the SSB (see Sec. III.B.2), however finite-size effects cause the imaginary part to vanish further than right after the critical point. Therefore, we illustrate the validity of Eq. (S80) only in the region where the imaginary part is negligible. Fig. S7 highlights the accuracy of Eq. (S80) as shown by the high fidelity between the steady-state obtained by numerical diagonalization of $\mathcal{L}_{\text{HEOM}}$ and the reconstructed steady-state $(\rho_+^{(\vec{0}, \vec{0})} + \rho_-^{(\vec{0}, \vec{0})})/2$. Although the \mathbb{Z}_2 symmetry is broken in phases (I) and (III), it is clear that the *way* it is broken is different. Indeed, the convergence is slower and less smooth in phase (III) than in phase (I). This can not be attributed to numerical errors due to a finite truncation order k_{max} since $\langle a \rangle = 0$ in phase (III) [see Eq. (S79)]. However, this could be due to the fact that in phase (I) it is the symmetry $S_x \rightarrow -S_x$, $a \rightarrow -a$ that is broken while in phase (III) it is the symmetry $S_y \rightarrow -S_y$. Interestingly, the former symmetry involves both the system and the environment, while the latter is more concerned with the coherent part of the generator. In this context, Fig.S7 suggests that the breaking of \mathcal{U}_2 through involving both the system and the pseudo mode is less prompt to undergo large finite-size effects.

VI. THIRD MODEL - CHALLENGING TWO-MODE DICKE MODEL

We now examine a two-mode Dicke model described by the Lindblad master equation [S11, S12]

$$\dot{\rho}_{\text{tot}} = -i[H, \rho_{\text{tot}}] + \kappa(\mathcal{D}[a] + \mathcal{D}[b]), \quad (S81)$$

where a, b are bosonic annihilation operators damped at rate κ and where

$$H = \omega_0 S_z + \omega_A a^\dagger a + \omega_B b^\dagger b + \frac{g}{\sqrt{N}}(aS_+ + bS_- + \text{h.c.}). \quad (S82)$$

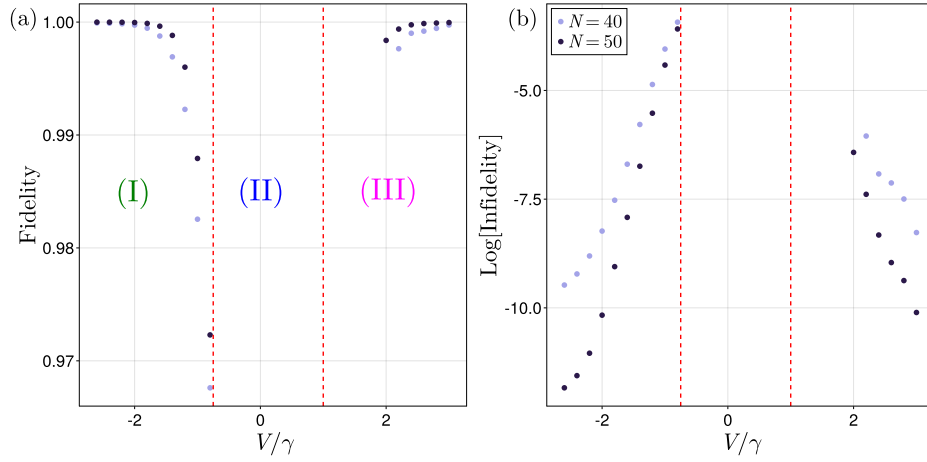


FIG. S7. Fidelity [(a)] and logarithm of the infidelity [(b)] (defined as $1 - F(A, B)$ for density operators A, B , with $F(A, B)$ as in Eq. (S70)) between the reconstructed state Eq. (S80) and the steady-state ρ_{ss} found by numerical diagonalization of $\mathcal{L}_{\text{HEOM}}$ for the second model as a function of V/γ in phases (I) and (III) for $N = 40, 50$ (see legend). Panels (a) and (b) prove the validity of the decomposition (S80). Note that we only show the region for which $\lambda_0^{(1)}$ is real ($\text{Im}[\lambda_0^{(1)}]/\omega < 10^{-8}$). The parameters are the same as those of Fig. 3 of the main text and $k_{\text{max}} = 9$.

This model undergoes a 2^{nd} -order DPT between a normal phase with $|\langle S_z \rangle| = N/2$ and a superradiant phase with $|\langle S_z \rangle| < N/2$ as $N \rightarrow \infty$ [S11]. For $\omega_A = \omega_B = \omega$, the critical value g_c of the coupling g that drives the transition can be calculated from a mean-field approach and satisfies $2g_c^2 N = \omega_0(\omega^2 + \kappa^2)/\omega$. The model (S81) exhibits a continuous $\mathbb{U}(1)$ symmetry described by $\mathcal{U}_1 = U_1 \otimes U_1^\dagger$ with $U_1 = e^{i\alpha(S_z + a^\dagger a - b^\dagger b)}$ ($\alpha \in \mathbb{R}$), spontaneously broken in the superradiant phase as $N \rightarrow \infty$.

Reduced descriptions of the spin dynamics have been studied and compared in [S12] with the mean-field results summarized above. It has been shown that, by contrast with the single-mode Dicke model [S10], a standard Redfield approach completely misses the DPT, while a 4^{th} -order Redfield master equation (i.e., a 4^{th} -order perturbative treatment of the interaction) captures the correct steady state and critical point but fails to predict the closing of the gap, a necessary condition for DPT. Our method, on the other hand, captures all features of the DPT and the SSB, as shown in Fig. S8, which displays the magnetization $\langle S_z \rangle$ (a), the closing of the gap $|\text{Re}[\lambda_0^{(k>0)}]|$ (c,d) and of the imaginary part of $\lambda_0^{(k>0)}$ (b), which have been obtained from the HEOM Liouvillian corresponding to Eq. (3) of the main text with $H_S = \omega_0 S_z$, $L_1 = S_-$, $L_2 = S_+$, $G_1 = G_2 = g^2/N$, $\omega_1 = \omega_2 = \omega$, $\kappa_1 = \kappa_2 = \kappa$.

VII. CONVERGENCE ANALYSIS AND NUMERICAL EFFICIENCY

The only parameter relevant to the convergence analysis of $\mathcal{L}_{\text{HEOM}}$ is the truncation order k_{max} . We introduce the following measures of convergence

$$\begin{aligned} C_{k_{\text{max}}}(O) &\equiv |\text{Tr}[\rho_{ss}(k_{\text{max}})O - \rho_{ss}(k_{\text{max}}+1)O]|, \\ S_{k_{\text{max}}}(\lambda) &\equiv |\lambda(k_{\text{max}}) - \lambda(k_{\text{max}}+1)|, \end{aligned} \quad (\text{S83})$$

to assess the convergence of $\mathcal{L}_{\text{HEOM}}$ with respect to the steady state expectation value of a given operator O or with respect to one of its eigenvalue λ , such as the HEOM Liouvillian gap. Here, $\rho_{ss}(k_{\text{max}})$ is the steady state of $\mathcal{L}_{\text{HEOM}}(k_{\text{max}})$ and similarly $\lambda(k_{\text{max}})$ is λ computed with $\mathcal{L}_{\text{HEOM}}(k_{\text{max}})$. Note that the convergence measure $C_{k_{\text{max}}}(O)$ is a natural choice often chosen to study the convergence of hierarchy of equations [S13]. The first part of this section is dedicated to the convergence analysis of $\mathcal{L}_{\text{HEOM}}(k_{\text{max}})$ while the second part shed light on the numerical advantage of $\mathcal{L}_{\text{HEOM}}$ over enlarged Markovian systems.

A. Convergence analysis of $\mathcal{L}_{\text{HEOM}}(k_{\text{max}})$

In Fig. S9, we show the two measures of convergence (S83) for the LMG model for $O = S_z$ [panels (a) and (b)] and $\lambda = \lambda_0^{(1)}$ [panels (c) and (d)]. As the hierarchy depth k_{max} increases, both measures of convergence $C_{k_{\text{max}}}(S_z)$

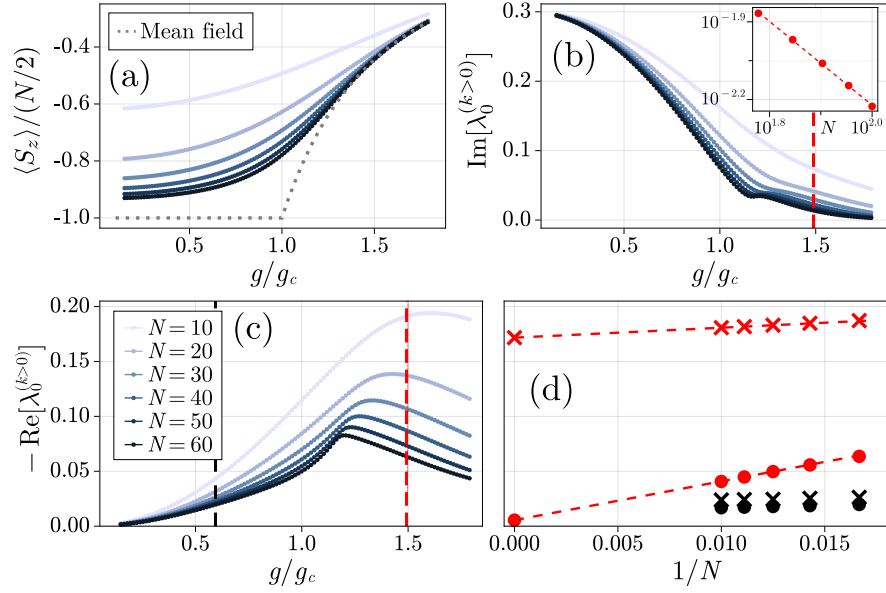


FIG. S8. Signatures of the 2^{nd} -order DPT for the two-mode Dicke model (S82) obtained from $\mathcal{L}_{\text{HEOM}}$ for $\kappa = \omega = 5\omega_0$. (a): Steady state magnetization $\langle S_z \rangle$ as a function of g for $N = 10-50$ ($k_{\text{max}} = 7$) and 60 ($k_{\text{max}} = 8$). As N increases, the curves get closer to the mean-field result (dotted line). (b) Imaginary part of the eigenvalue $\lambda_0^{(k>0)}$ with the largest real part among all symmetry sectors with $k > 0$ as a function of g/g_c , confirming the SSB. The inset shows the scaling of $\text{Im}[\lambda_0^{(k>0)}]$ as a function of N at $g/g_c = 1.49$. (c) $-\text{Re}[\lambda_0^{(k>0)}]$ as a function of g/g_c showing a decreasing gap in the superradiant phase as N increases. The vertical dashed lines show $g/g_c = 1.49$ (red) and $g/g_c = 0.6$ (black) used in panel (d) to compare the scaling of $-\text{Re}[\lambda_0^{(k>0)}]$ (circles) and of the Liouvillian gap of the 4th Redfield master equation of [S12] (crosses) as a function of $1/N$ [with $N = 60-90$ ($k_{\text{max}} = 8$) and 100 ($k_{\text{max}} = 9$)]. In the normal phase (black), both methods are in good agreement, while in the superradiant phase (red), only $\mathcal{L}_{\text{HEOM}}$ gives the expected closing. The points at $1/N = 0$ were extrapolated from a line defined by the two last points of our data.

and $S_{k_{\text{max}}}(\lambda_0^{(1)})$ globally decrease, showing that the truncation order k_{max} can be used to control the numerical errors inherent to the $\mathcal{L}_{\text{HEOM}}(k_{\text{max}})$ scheme. A comparison of the panels (a) and (c) with the panels (b) and (d) indicates that errors scale up as N increases. We also note that it is numerically more challenging to extract the spectral quantity $\lambda_0^{(1)}$ than the steady state expectation value $\langle S_z \rangle$, as indicated by the change in scale on the y-axis between panels (a) and (c) or (b) and (d).

These general observations still hold for the $\text{U}(1)$ -symmetric Dicke model, as illustrated in Fig S10, which is the analog of Fig S9 but for the $\text{U}(1)$ -symmetric Dicke model. We note that both $C_{k_{\text{max}}}(S_z)$ and $S_{k_{\text{max}}}(\lambda_0^{(k>0)})$ increases as the coupling g increases, highlighting the numerical challenge of the so-called strong coupling regime. Moreover, this observation combined with the fact that the computation of $\lambda_0^{(k>0)}$ is numerically more demanding than that of $\langle S_z \rangle$ could explain why a fourth order Redfield master equation seems to capture the right steady state but predicts a non-vanishing gap [S12]. We indeed foresee that the spectrum of $\mathcal{L}_{\text{HEOM}}$ converges faster for larger eigenvalues.

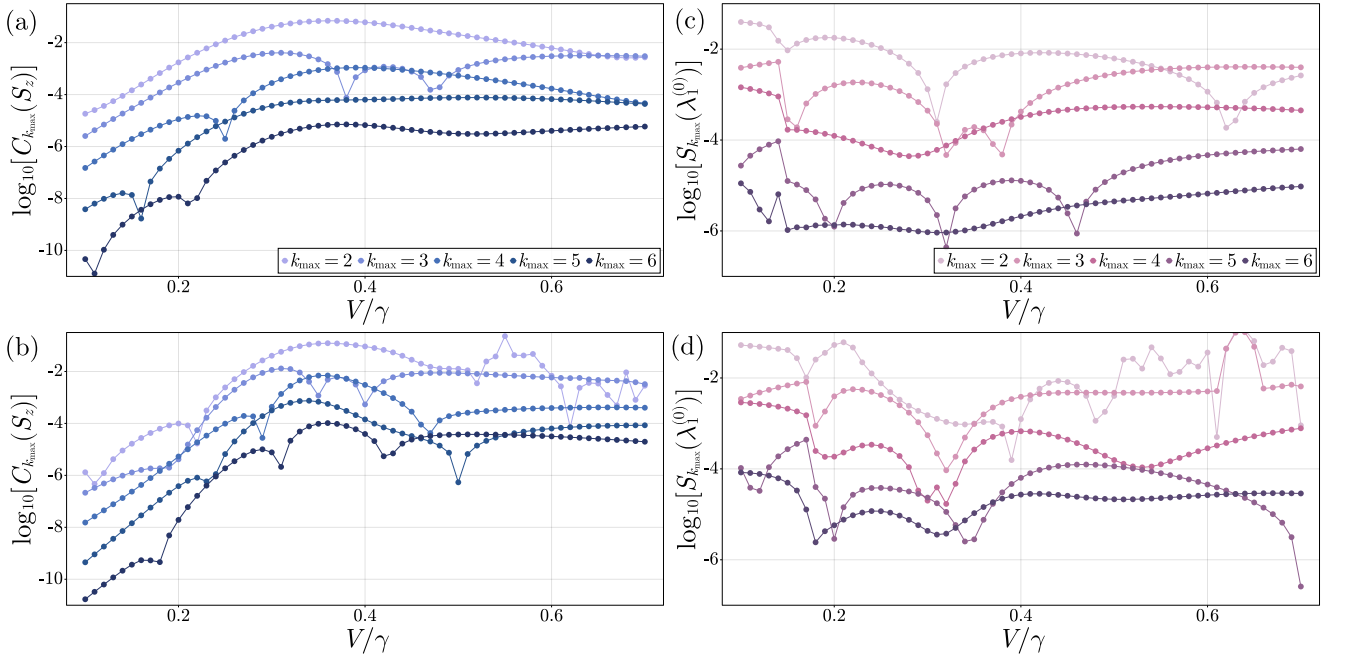


FIG. S9. Measures of convergence $C_{\max}(S_z)$ and $S_{k_{\max}}(\lambda_1^{(0)})$ as defined by Eq. (S83) for the LMG model discussed in the main text displayed in logarithmic scale as a function of V/γ . For all plots, the parameters are $\kappa = \omega = \gamma$ and $N = 10$ for panels (a) and (c) and $N = 20$ for panels (b) and (d).

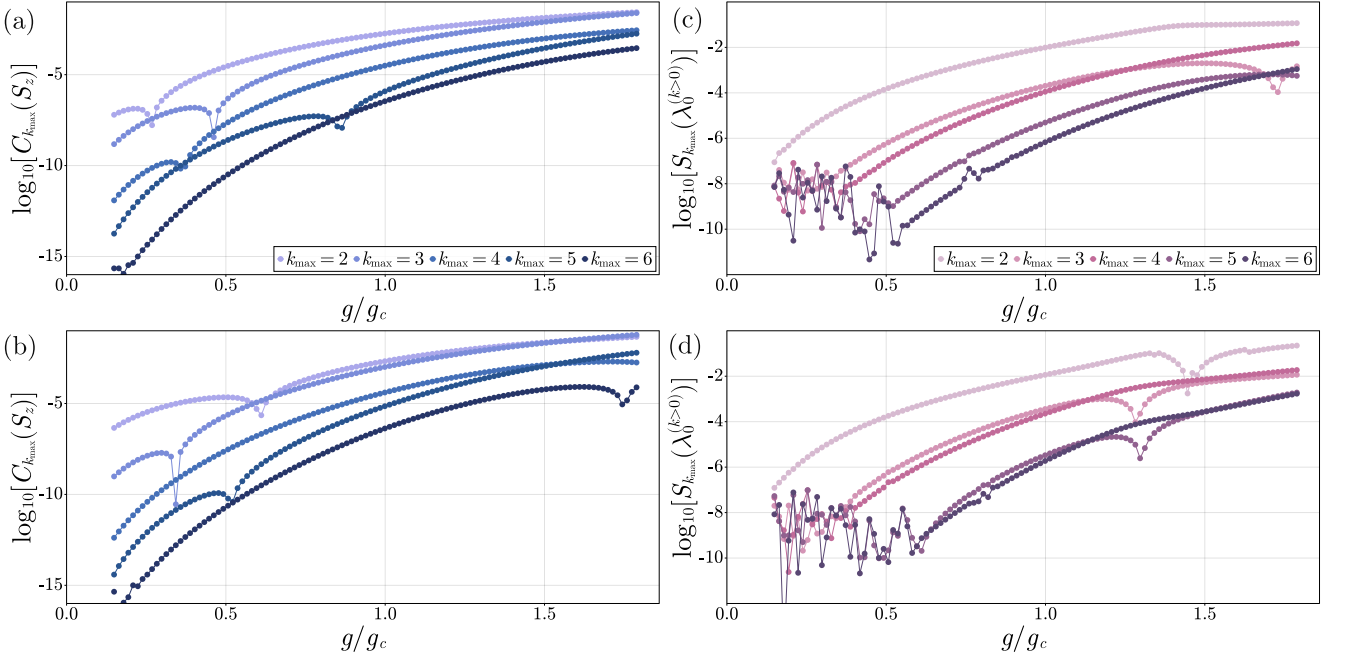


FIG. S10. Measures of convergence $C_{\max}(S_z)$ and $S_{k_{\max}}(\lambda_1^{(0)})$ as defined by Eq. (S83) for the U(1)-symmetric Dicke model discussed in Sec. VI displayed in logarithmic scale as a function of V/γ . For all panels, the parameters are $\kappa = \omega = 5\omega_0$ and $N = 10$ for panels (a) and (c) and $N = 20$ for panels (c) and (d).

B. Comparison with enlarged Markovian systems

Let us illustrate the numerical advantage of our method to characterize DPTs over the standard technique of analysing the spectrum of the Liouvillian for the enlarged Markovian system of the first model considered in the main text. For this model, this Markovian Liouvillian superoperator \mathcal{L}_M is defined through

$$\dot{\rho}_{\text{tot}} = -i[H, \rho_{\text{tot}}] + \kappa(2a\rho_{\text{tot}}a^\dagger - \{a^\dagger a, \rho_{\text{tot}}\}) \equiv \mathcal{L}_M[\rho_{\text{tot}}]. \quad (\text{S84})$$

where $H = H_{\text{LMG}} + \omega a^\dagger a + \sqrt{\frac{\gamma\kappa}{2N}}(S_- a^\dagger + S_+ a)$. As the dimension of \mathcal{L}_M is infinite, one has to introduce a cutoff in order to determine the steady state of \mathcal{L}_M numerically. We denote by N_c and $\mathcal{L}(N_c)$ the effective dimension of the truncated Fock space of the pseudo-mode and the associated truncated Markovian Liouvillian. In order to compare \mathcal{L}_M and $\mathcal{L}_{\text{HEOM}}$, we fix a threshold of tolerance for the measures of convergence, namely $\epsilon = 0.001$. We then choose k_{max} and N_c accordingly: we take the first value of k_{max} and N_c that satisfy

$$C_{k_{\text{max}}}(S_z) < \epsilon \quad \text{and} \quad C_{N_c}(S_z) \equiv |\text{tr}(\rho_{ss}(N_c)S_z - \rho_{ss}(N_c + 1)S_z)| < \epsilon, \quad (\text{S85})$$

where $\rho_{ss}(N_c)$ is the steady state associated with $\mathcal{L}_M(N_c)$. We then compute the effective dimension of \mathcal{L}_M and $\mathcal{L}_{\text{HEOM}}$ for the truncation parameters k_{max} and N_c previously determined. Figure S11(a) shows that the ratio $\text{dim}(\mathcal{L}_{\text{HEOM}})/\text{dim}(\mathcal{L}_M)$ is below 0.4 for all V/γ and N considered. Moreover, this ratio decreases with N , which shows that the $\mathcal{L}_{\text{HEOM}}$ scheme is more suited for the study of DPTs for which one must consider the thermodynamic limit $N \rightarrow +\infty$. Let us finally mention that the generators $\mathcal{L}_{\text{HEOM}}$ and \mathcal{L}_M give the same results at the chosen tolerance threshold as illustrated in Fig. S11(b).

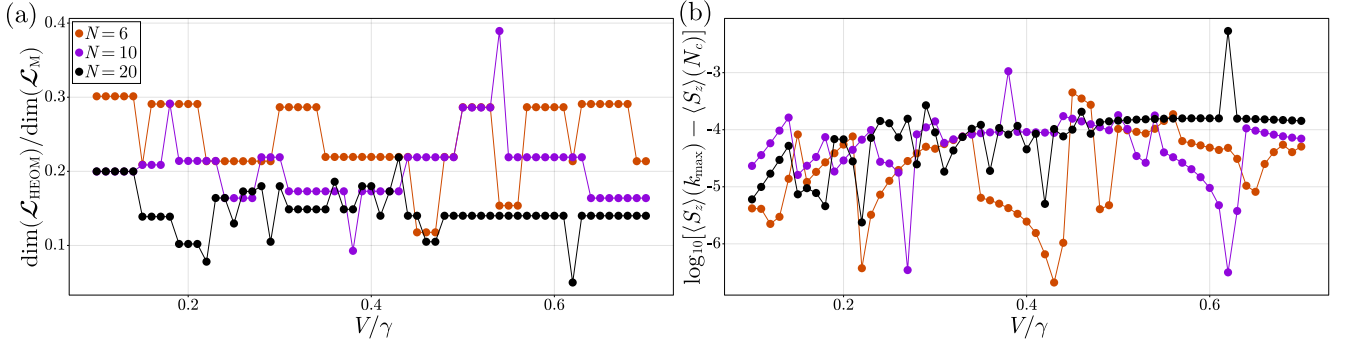


FIG. S11. Comparison of the convergence of $\mathcal{L}_{\text{HEOM}}$ and \mathcal{L}_M . (a): Ratio between the dimension of the HEOM generator $\mathcal{L}_{\text{HEOM}}$ and the Markovian one \mathcal{L}_M as a function of V/γ for $\epsilon = 0.0001$, proving the numerical gain of using $\mathcal{L}_{\text{HEOM}}$ instead of \mathcal{L}_M for the enlarged Markovian system. (b): Differences in logarithmic scale between the steady state expectation value $\langle S_z \rangle$ computed with $\mathcal{L}_{\text{HEOM}}(k_{\text{max}})$ (resp. $\mathcal{L}_M(N_c)$) denoted by $\langle S_z \rangle(k_{\text{max}})$ (resp. $\langle S_z \rangle(N_c)$) for $\epsilon = 0.0001$. The two methods are in good agreement at the given tolerance.

-
- [S1] M. Zwolak and G. Vidal, Phys. Rev. Lett. **93**, 207205 (2004).
[S2] V. Link, K. Müller, R. G. Lena, K. Luoma, F. Damanet, W. T. Strunz, and A. J. Daley, PRX Quantum **3**, 020348 (2022).
[S3] F. Minganti, A. Biella, N. Bartolo, and C. Ciuti, Phys. Rev. A **98**, 042118 (2018).
[S4] T. Kato, *Perturbation theory for linear operators* (Springer, 1995).
[S5] J. Huber, P. Kirton, and P. Rabl, Phys. Rev. A **102**, 012219 (2020).
[S6] T. E. Lee, C.-K. Chan, and S. F. Yelin, Phys. Rev. A **90**, 052109 (2014).
[S7] H.-P. Breuer and F. Petruccione, *The Theory of Open Quantum Systems* (Oxford University Press, Oxford, 2006).
[S8] P. Ribeiro, J. Vidal, and R. Mosseri, Phys. Rev. E **78**, 021106 (2008).
[S9] N. Debergh and F. Stancu, Journal of Physics A: Mathematical and General **34**, 3265 (2001).
[S10] F. Damanet, A. J. Daley, and J. Keeling, Phys. Rev. A **99**, 033845 (2019).
[S11] R. I. Moodie, K. E. Ballantine, and J. Keeling, Phys. Rev. A **97**, 033802 (2018).
[S12] R. Palacino and J. Keeling, Phys. Rev. Research **3**, L032016 (2021).
[S13] D. Suess, A. Eisfeld, and W. T. Strunz, Phys. Rev. Lett. **113**, 150403 (2014).